Chapter 9
Gold and Silver Fluorescent Nanomaterials as Emerging Probes for Toxic and Biochemical Sensors

Nagamalai Vasimalai and Maria T. Fernandez-Argüelles

Abbreviations

AB	Amido black 10B
AChE	Acetylcholinesterase
ACTI	S-acetylthiocholine iodide
AgNCs	Silver nanoclusters
AgNDs	Silver nanodots
ALP	Alkaline phosphatase
AP	Apoferritin
APTES	(3-aminopropyl)triethoxysilane
AuNCs	Gold nanoclusters
AuNDs	Gold nanodots
AuNRs	Gold nanorods
BPA	Bisphenol A
BSA	Bovine serum albumin
C-dots	Carbon dots
cfu/mL	Colony-forming unit per milliliter
ChOx	Cholesterol oxidase
CK2	Protein kinase II
CSFs	Cerebrospinal fluids
dBSA	Denatured BSA
DHLA	Dihydroxylipoic acid
DNA	Deoxyribonucleic acid
ds	Double stranded

N. Vasimalai (✉) • M.T. Fernandez-Argüelles
INL – International Iberian Nanotechnology Laboratory, Av. Mestre José Veiga, 4715-330, Braga, Portugal
e-mail: vasimalai.gri@gmail.com; vasi.malai@inl.int

F.L. Deepak (ed.), *Metal Nanoparticles and Clusters*,
https://doi.org/10.1007/978-3-319-68053-8_9

E. coli	*Escherichia coli* bacteria
EDC	1-ethyl-3-(3-dimethylaminopropyl)carbodiimide
EDTA	Ethylenediaminetetraacetic acid
eV	Electron volt
FITC	Fluorescein isothiocyanate
FRET	Forster resonance energy transfer
GOD	Glucose oxidase
GSH	Glutathione
GST	Glutathione S-transferase
h	Hours
HAS	Human serum albumin
HH	Human hemoglobin
HOCl	Hypochlorous acid
HOMO	Highest occupied molecular orbital
L-AAO	L-amino acid oxidase
L-DOPA	L-3,4-dihydroxyphenylalanine
LED	Light-emitting diode
LOD	Lowest detection limit
LUMO	Lowest unoccupied molecular orbital
Man	11-mercapto-3,6,9-trioxaundecyl-r-D-mannopyranoside
μg	Microgram
MIP	Molecular-imprinted polymer
mL	Milliliter
μm	Micrometer
mM	Millimolar
MRSA	Methicillin-resistant *Staphylococcus aureus*
NAD^+	Oxidization form of NADH
NADH	1,4-dihydronicotinamide adenine dinucleotide
NCs	Nanoclusters
NDs	Nanodots
NHS	N-Hydroxysuccinimide
NIR	Near infrared
nm	Nanometer
nM	Nanomolar
PBS	Phosphate buffer solution
PDDA	Poly diallyldimethyl ammonium chloride
PDMAM	Poly(N,N′-methylenebisacrylamide)
PPi	Pyrophosphate
QY	Quantum yield
S.E.M	Standard error measurements
SEM	Scanning electron microscope
SPEET	Surface plasmon-enhanced energy transfer
ss	Single stranded
TEM	Transmission electron microscopy
TEOS	Tetraethyl orthosilicate
THPC	Tetrakis(hydroxymethyl)phosphonium chloride

TMB	3,3′,5,5′-tetramethylbenzidine
TNT	2,4,6-trinitrotoluene
US EPA	US environmental protection agency
UV	Ultraviolet
UV-vis	Ultraviolet-visible
λ_{em}	Emission wavelength
λ_{ex}	Excitation wavelength
μM	Micromolar

9.1 Introduction

Our world is facing serious threats caused by air, soil, and water pollution. In addition to the shortage of water, production of large volumes of wastewater has put a lot of pressure on humankind [1, 2]. On the other hand, the detection of biological molecules including amino acids, vitamins, and proteins is also important in different areas including biology, medicine, food industry, etc. [1–3]. Therefore, it is very important to perform monitorization of these toxic and biological compounds via portable sensing devices, which encompass the demand of being low cost and the potential for online environmental monitoring and food safety applications. Currently, a wide variety of techniques have been used for the detection of biochemical and toxic compounds including UV-vis absorption spectroscopy [4], ion exchange chromatography [5], inductively coupled plasma mass spectrometry [6], voltammetry [7], mass spectrometry [8], atomic absorption spectrometry [9], calorimetry [10], high-performance liquid chromatography, etc. [11]. However, these methods have some demerits that typically include high cost, long analysis time, need of trained personnel to operate the instrument, tedious procedures, etc.

On the other hand, the optical sensors are analytical devices that can detect the target analyte based on changing their optical properties, such as absorbance or photoluminescence. While compared to the absorbance-based sensor, fluorescent-based sensors are 1000-fold more sensitive. This is a powerful technique for environmental monitoring, molecular recognition, and medical diagnosis applications. In general terms, when a fluorophore absorbs light with a particular wavelength (excitation wavelength), it is able to emit energy in a form of fluorescence equal to the energy difference between the excited state and the ground state. Mostly organic dyes and semiconductor quantum dots (CdS, CdSe, and ZnS) are used as fluorophores in the sensor devices. However, these materials often suffer from poor photostability and also toxicity of heavy metals. Moreover, most of the organic dyes and semiconductor nanomaterials are soluble only in organic solvents, which is an important drawback for the development of optical sensors that will be used in aqueous media [12, 13].

In the last few years, researchers have been developing new nanomaterials to be used in different areas including electronics, solar cells, cancer diagnosis, catalysis, sensing, etc. Among them, gold and silver fluorescent nanoclusters (NCs) and nanodots (NDs) have gained momentum due to their unique and intrinsic physical and chemical properties, such as small size [14–16], discrete electronic transitions

[17, 18], molecular-like structure [19–22], quantized charging [23], optical chirality [19, 24, 25], and strong photoluminescence [22, 26, 27].

In 1969, fluorescent properties of metallic gold were observed for the first time by Mooradian [28]. Gold and silver nanoparticles show a size-dependent plasmon absorption band when their conduction electrons in both the ground and excited states are confined to dimensions smaller than the electron mean free path (ca 20 nm). But plasmon absorption disappears completely for nanoparticles smaller than 2 nm, where Mie's theory no longer can be applied [14]. Size-dependent fluorescence of Au/AgNCs is related to the energy difference between highest occupied molecular orbital (HOMO) and lowest unoccupied molecular orbital (LUMO) [14], whereas other reports indicate that the fluorescence of molecular-like AuNCs occurs at lower energy than the HOMO-LUMO gap energy [29]. It has been also suggested that the fluorescent properties of Au/AgNCs are attributed to recombination involving d-band excitation [30]. The absorbed photons promote electrons from the narrow d-band to the empty sp band above the Fermi level. Radiative recombination responsible for the emission occurs between electrons and excited holes when some carriers relax, resulting in visible-NIR fluorescence emission [30].

Gold nanodots (AuNDs) are also a new class of fluorescent gold nanomaterials and are of great interest for researchers. Because of their interesting properties including high photoluminescence, biocompatibility, good stability, facile preparation, ultrasmall size, etc. [31, 32]. Nanodots are the bridge between nanoclusters and nanoparticles, displaying molecular-like properties [31]. The NDs also exhibit fluorescence emission in the visible to NIR region [32]. Hence, they are attractive materials to be explored in fields including biosensors, bioimaging, drug delivery, solar cells, light-emitting diode (LED), etc.

Commonly, the emission wavelengths of NCs and NDs are associated to the stabilizing ligands surrounding on their surface [14]. In fact, the surface ligands play a major role in enhancing the fluorescence of thiol-protected NCs and NDs in two ways:

1. The charge transfer from the ligands to the gold or silver core through the Au-S or Ag-S bonds
2. The direct donation of delocalized electrons from electron-rich atoms or groups of the ligands to the gold or silver metal core

It is well known that the fluorescence of NCs or NDs is dependent on capping ligands, size of the particle, solvent medium, etc. Less than 2 nm size of NCs or NDs exhibits the emission from blue to red region. For example, blue emittive AuNCs were prepared by using DNA (5′-CCCCCCCCCCCCTTTTTT-3) ligand [33]. The purine-AuNDs exhibited the green fluorescence [34], and BSA-AuNCs and DHLA-AuNCs showed the red fluorescence [35, 36]. Orange-yellow fluorescent AuNCs were synthesized and capped with homocysteine [37]. Mercaptosuccinic acid-protected Ag_7 and Ag_8 NCs were prepared by etching of AgNPs, and have shown the blue and red emission, respectively [38]. Zheng et al. reported the different sizes of poly(amidoamine)dendrimer (PAMAM)-templated AuNCs (PAMAM-AuNCs), such as Au_5, Au_8, Au_{13}, Au_{23}, and Au_{31} atom size of PAMAM-AuNCs. These

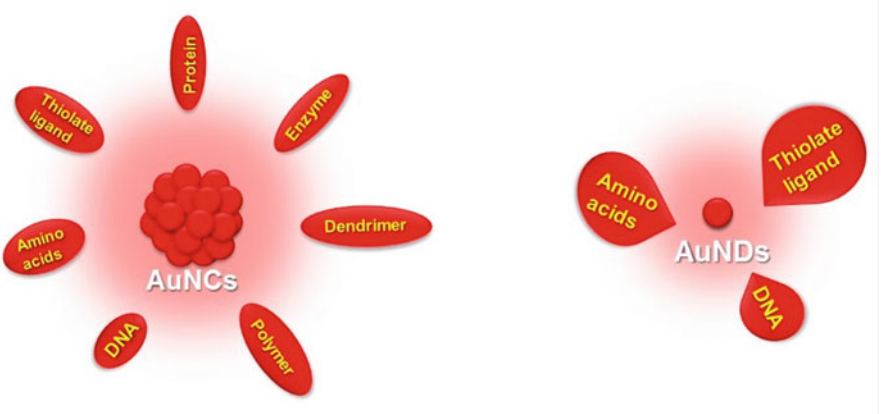

Scheme 9.1 Schematic representation of the ligand shell metal core structure of AuNCs and AuNDs protected by different ligands

AuNCs displayed the UV (385 nm), blue (455 nm), green (510 nm), red (760 nm), and red (866 nm) fluorescence, respectively [32, 39]. These reports revealed that the fluorescence of gold nanomaterials is highly sensitive with surface-capped ligands, size and solvent medium [40].

Commonly, NCs are prepared by thermal reduction, microwave heating, photoreduction, metal core etching by ligand, and template-assisted and sonochemical methods. As shown in Scheme 9.1, NCs and NDs can be prepared by using different ligands. For example, the NC metal atoms can be covered by ligands such as DNA, proteins, enzymes, polymers, thiolated ligands, etc. The ND syntheses are two types such as etching and direct synthesis methods. For the general synthesis (etching method) of NDs, tetrakis(hydroxymethyl)phosphonium chloride (THPC)-capped gold nanoparticles (THCP-AuNPs) are used to be etched by thiolated ligands. For direct synthesis of NDs, researchers commonly used thiolated ligands to prepare NDs by mixing with gold chloride. In this case, the thiolated ligands can act as capping as well as reducing agent. Scheme 9.1 illustrates the schematic representation of AuNCs and AuNDs protected by different ligands. In addition, these ligands also considerably contribute to the physical and chemical properties of NC and NDs. Both metal core and ligand can interact with the analytes, giving rise to changes on the luminescent signals, a feature exploited in the development of fluorescent (bio)chemical sensors [41].

Therefore, the synthesis of highly luminescent Au/AgNCs and NDs with suitable surface modifications to develop fluorescent sensors or fluorescent sensing probes for the detection of biochemical compounds is a field of great interest nowadays. In this chapter, we briefly summarize the main routes for Au/AgNC and ND synthesis, and we review the latest fluorescent sensing applications for detection of a wide range of different analytes, including biomolecules or contaminants with an emphasis on the sensing mechanism.

9.2 Synthetic Methods of Gold and Silver Nanoclusters

In general, the smaller size of metal NCs can easily agglomerate and produce nonfluorescent larger nanoparticles. Ultimately, there are two main routes for the synthesis of gold and silver NCs: bottom-up and top-down strategies. In bottom-up method, Au/AgNCs are obtained typically based on the use of a metal ion as a precursor in solution form. Further, a different size of particle and also some fascinating properties of the NCs can be obtained by simply altering the experimental conditions [42], including selection of reducing agent and variation of molar ratio of components, the metallic salt, capping ligands, temperature, pH, reaction time, etc. [43]. Frequently, proteins, DNA, enzymes, mercapto-functionalized polymers, and thiolated compounds are utilized as capping as well as stabilizing agents for metal NCs due to their strong affinity with Au or Ag as illustrated in Scheme 9.1. Further, strong and mild reducing agents including sodium borohydride, hydrazine hydrate, ascorbic acid, and THPC are most frequently employed depend upon the necessity of individual condition. Interestingly, it was found that certain mild reducing agents including citrate, glutathione (GSH), trithiocyanuric acid, D-penicillamine, etc. act as both reductant and capping agents [42, 44]. Moreover, apart from the use of reducing agent, some other protocols are also routinely employed to synthesize metal NCs by bottom-up method including template-assisted, photoreduction, ultrasonic, microwave-assisted, and solid-phase synthesis [45].

Conversely, syntheses of metal NCs by top-down strategies are mainly based on an etching approach. In this method, the smaller size of metal NCs can be obtained by etching of large size particles with amino and mercapto-functionalized ligands due to the sturdy interaction of metal core with ligand [35]. For instance, polyethylenimine (PEI), mercaptosuccinic acid (MSA), 11-mercaptoundecanoic acid (11-MUA), mercaptohexanol, GSH, and BSA are commonly used to perform metal nanoparticle etching [42, 45]. The main advantage of this technique is that it is very simple and effective, and also the obtained smaller size nanoparticles are extremely stable due to the absence of any harmful strong reducing agents in the process.

9.3 Bio- and Toxic Chemical Sensing by Luminescent Au/Ag Nanomaterials

In the last decade, metal NCs have been extensively explored as probes for the detection of several vital compounds including biomolecules, inorganic and organic toxicants, cations and anions, etc. The metallic NCs are highly reactive, giving rise to improved sensitivity and selectivity due to their ultrasmall size, higher surface area, and most importantly, the functionalization with different capping ligands. Hence, in this section, we aim to summarize the recent developments and applications of NCs based on their interesting luminescence properties toward the

detection of various analytes including cations and anions, biomolecules, small molecules, toxic compounds, and bacteria.

It was reported that Ag/AuNCs show a magnificent fluorescence signaling with their interaction with analytes. Basically, the fluorescent sensors are divided into two types such as on-off and off-on. So far there are six sensing mechanisms reported for the detection of various analytes [41, 46, 47] as described below:

1. Metallophilic interaction
2. Interaction with metal core
3. Ligand-induced aggregation
4. Ligand-induced charge transfer
5. Ligand decomposition
6. Indirect approach

These six sensing mechanisms are discussed in details with relevant examples as follows. In metallophilic (metal-metal) interaction, a bond formation takes place between two metal ions such as analyte metal ions and NCs. For example, an analyte Hg^{2+} ($5d^{10}$) forms a bond with NCs Au^{+} ($5d^{10}$), and this bond formation (Hg^{2+}-Au^{+}) can effectively change the fluorescent properties of NCs. The second mechanism is analyte interaction with metal core. In this case, an analyte can interact with a metal core by etching process as it is found that CN^{-} ion can interact with AuNCs to form strong Au-CN complex, and it obviously leads to quench the fluorescence of AuNCs. In ligand-induced aggregation mechanism, the surface ligand which is attached on the metal surface for stabilizing purposes can induce the aggregation of NCs while interacting with analytes. It was observed that the carboxylate functionalized ligand-capped NCs can effectively interact with cations through electrostatic interaction to form a complex, which could induce the aggregation of NCs. Similarly, in the ligand-induced charge transfer mechanism, the charge transfer can occur via Au-S bonding. As a result, the charge transfer induced the selective binding of analytes with ligands.

In contrast, in the ligand decomposition mechanism, a small or macromolecule with thiol or amine functionalization can protect the NCs from aggregation by electrostatic effect with their counterion charge or steric effect of their bulky functional groups. However, sometimes the liberation of capped ligands may occur due to the analyte interaction with the metal core and replaced capping agent. Finally, the indirect approach is one of the interesting methods. In this method, the competitive binding force is playing an important role. As discussed earlier, in metallophilic interaction, Hg^{2+} ion can form a bond with NCs (Hg^{2+}-Au^{+}), and it leads to aggregation. Interestingly, the use of aggregation complex a target analyte (e.g., GSH) can be detected indirectly as a result of formation of competitive coordination of analyte (GSH) between Hg^{2+} and NCs [41, 46, 47].

9.3.1 Detection of Cations and Anions

A very important source of water pollution is caused by disposal of heavy metal ions from industrial effluents. Further, these heavy metal ions can bind to different

Table 9.1 The permissible level of toxic ions in drinking water by US EPA and their potential health effects

Toxic ions	US EPA permissible level	Potential health effects
Hg^{2+}	10.07 nM	Kidney disease
Cd^{2+}	45.29 nM	Kidney disease
Pb^{2+}	73.09 nM	Kidney disease and high blood pressure
As^{3+}	0.14 μM	Skin allergy and potential increased risk of cancer
Cu^{2+}	21.13 μM	Gastrointestinal distress and liver or kidney disease
Ag^{+}	0.94 μM	Skin discoloration and cornea disease in eyes
Cr^{3+}	2.00 μM	Allergic dermatitis
CN^{-}	7.40 μM	Thyroid and neurological problems
Cl^{-}	27.39 μM	Neurological problems and anemia
NO_2^{-}	0.21 mM	Blue baby syndrome and shortness of breath
S^{2-}	0.23 μM	Respiratory paralysis and irritation of the mucous membranes

cellular components including nucleic acids, enzymes, proteins, etc., leading to changes on their biological functions. For example, bivalent heavy metal ions such as Hg^{2+}, Pb^{2+}, Cu^{2+}, Cd^{2+}, etc. can strongly bind with the amino acid backbone of enzymes, and it can inhibit the enzymatic activity. It has been reported that the high concentrations of heavy metal ions such as Hg^{2+}, Pb^{2+}, Cd^{2+}, Cu^{2+}, As^{3+}, Ag^{+}, Cr^{3+}, Cr^{6+}, and Fe^{2+} or other toxic anions such as CN^{-}, NO_2^{-}, I^{-}, Cl^{-}, S^{2-}, etc. are a serious threat to the environment and living beings. The US Environmental Protection Agency (US EPA) recommends a maximum accepted level of these ions in drinking water [48], and related diseases are caused by exceeded metal ion levels which are summarized in Table 9.1.

Therefore, in recent years, the researchers are highly focusing on the development of sensing probes and strategies to detect these toxic ions (Table 9.1). Among these toxic ions, researchers are paying more attention for the sensing of Hg^{2+} due to its abundance in the environmental water from different sources. The detection of Hg^{2+} has been reported by Huimin Ma and co-workers, and they successfully employed the detection of Hg^{2+} in tap and river water [49]. For the mercury sensor probe, first, they synthesized enzyme-capped AuNCs by simple mixing of aqueous $HAuCl_4$ and L-amino acid oxidase (LAAOx) and incubated at 37 °C for 12 h. Interestingly, L-amino acid oxidase-capped AuNCs (L-AAO-AuNCs) show red emission with an emission maximum at 630 nm while excited at 510 nm. As mentioned before, while adding Hg^{2+} in the reaction mixture immediately, mercury ion forms strong metal-metal bond with Au^{+} via metallophilic interaction (Hg^{2+}-Au^{+}). As a result, the fluorescence quenching was observed at 630 nm and it enables the detection of Hg^{2+}. Further, it was found that this method is highly sensitive and the detection limit was found to be 58 nM. Subsequently, dual sensor was developed for Hg^{2+} and oxytetracycline with dual ligands threonine and 11-MUA-capped AuNCs (T@MUA-AuNCs) by turn-off and turn-on mechanism [50]. First, MUA was dissolved with NaOH and allowed to stir, and then gold chloride solution was added into the reaction mixture. After 1.5 h of stirring, the solution was filtered

with 0.22 μm filter paper. The obtained AuNC size was calculated to be 1.8 nm, and it shows an emission maximum at 606 nm with an excitation wavelength of 282 nm. The emission intensity of T@MUA-AuNCs was quenched (turn-off) upon addition of Hg^{2+} ion into T@MUA-AuNCs. Based on decreasing emission intensity the concentration of Hg^{2+} was quantified and the detection was achieved to be 0.357 μM. Conversely, the intensity of fluorescence was increased, while addition of another analyte oxytetracycline to the Hg^{2+}-T@MUA-AuNC complex is associated with the turn-on mechanism. Hence, the enhancement of fluorescence allows to determine oxytetracycline concentration, and a detection limit obtained 12.5 μM. Finally, this sensor was successfully applied to detect the oxytetracycline in human serum samples.

Interestingly, dual emittive probe was developed for Hg^{2+} sensor. Blue emittive carbon dots (C-dots) were prepared from L-proline by hydrothermal method. The diameter of C-dots was found to be 2.2 nm by TEM. Again the red emittive (2 nm size) BSA-AuNCs were synthesized by wet chemical method [51]. Then, BSA-AuNCs were coupled with C-dots by simple mixing and allowed to be stirred in order to obtain C-dots@BSA-AuNCs (nanohybrid system), which show dual emission maximum at 450 and 656 nm with an excitation wavelength of 365 nm and exhibit a red color under UV light (Fig. 9.1a). The observed emission intensity at 450 nm and 656 nm attributed to the C-dots and BSA-AuNCs, respectively. After the addition of Hg^{2+} into C-dots@BSA-AuNCs, the emission intensity at 656 nm was quenched without any fluorescence change at 450 nm as depicted in Fig. 9.1a.

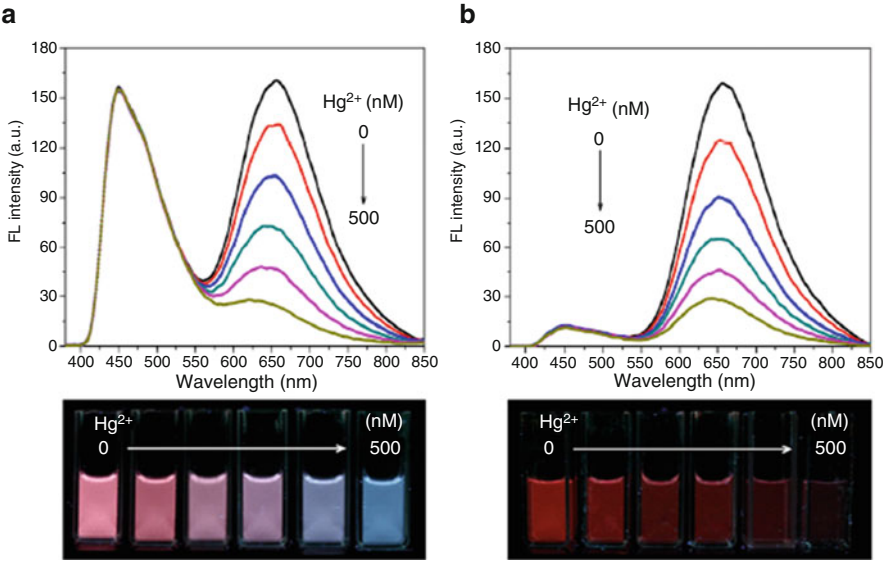

Fig. 9.1 The fluorescence spectra of (**a**) the nanohybrid system and (**b**) the sole red AuNCs, in the presence of Hg^{2+} (0.0, 100, 200, 300, 400, and 500 nM). *Bottom*: fluorescence images of the probe solution in the presence of various amounts of Hg^{2+} recorded under a 365 nm UV lamp (Reprinted by permission from Springer: [Nano Research] 9(7), 2088–2096, Copyright 2016)

Moreover, significantly the color of the solution also changed from red to blue. This apparently indicates the new complex formed by binding of Hg^{2+} with BSA-AuNCs. The sole BSA-AuNCs show the weak fluorescence quenching. In this case, the red emission becomes completely quenched after the addition of Hg^{2+}, and it is hard to be distinguished by naked eye view (Fig. 9.1b). Finally, the C-dots@BSA-AuNCs were utilized for the detection of Hg^{2+} in mineral, lake, and tap water samples and achieved a detection limit of 28 nM. Further, paper based calorimetric sensor of Hg^{2+} also was demonstrated. This dual emittive system enhanced the sensitivity, and the detection limit reached to nanomolar level.

Again, 2.1 nm size of BSA-AuNCs were prepared by microwave-assisted method and successfully used as probe for the detection of Hg^{2+} by Hsu et al. [52]. It has been reported that the BSA-AuNCs show an emission maximum at 650 nm with an excitation wavelength at 350 nm, with a quantum yield of 1.9%. The detection of Hg^{2+} was performed at pH 7 in 4-(2-hydroxyethyl)-1-piperazineethanesulfonic acid buffer. The fluorescence of BSA-AuNCs was quenched after addition of Hg^{2+}, achieving a detection limit of 2.98 nM. Interestingly, the quenched luminescence was enhanced after the addition of $NaBH_4$ due to the formation of metallic Hg and liberation of free BSA-AuNCs. Peptide-AuNCs (P-AuNCs) with size of 1.2 nm also were used as probe for Hg^{2+} determination, and they show an emission maximum at 650 nm upon excitation at 365 nm. Due to the strong affinity of Hg^{2+} with Au^{+}, the fluorescence was quenched after the addition of Hg^{2+} into P-AuNCs. The usual common interferents such as K^{+}, Mg^{2+}, Ca^{2+}, Pb^{2+}, Ni^{2+}, Fe^{3+}, Cu^{2+}, and EDTA did not show any effect on the signal. The metal chelating agent of EDTA with high concentration (Hg^{2+}/EDTA ratio, 1:50) also did not interfere in this system, and the detection limit of 7.5 nM was achieved [53].

Further, the blue emittive DNA (5′-CCCCCCCCCCCCTTTTTT-3)-capped AuNCs (DNA-AuNCs) also were employed to detect Hg^{2+} [33]. Due to the binding of Hg^{2+} through the formation of thymidine-Hg^{2+}-thymidine duplexes, the fluorescence of the DNA-AuNCs was quenched, and aggregation of DNA-AuNCs was observed by TEM. Based on the fluorescence quenching of DNA-AuNCs, the detection limit was reported to be 8.3 nM, and the probes were successfully evaluated in lake water and human urine samples. Chang et al. reported that the synthesis of green emittive Ag-thiosulfate capped BSA-AgNCs ($Ag(S_2O_3)_2$@BSA-AgNCs) [54]. It is known that during the synthesis of AgNCs in alkali medium, Ag^{+} can precipitate on the bottom of the beaker. To avoid the Ag^{+} precipitation, the silver complex $[Ag(S_2O_3)_2]_3^{-}$ was prepared by mixing $AgNO_3$ and $Na_2S_2O_3$ solution. Upon the addition of BSA, the $[Ag(S_2O_3)_2]_3^{-}$ was reduced to Ag^0 and formed a stable BSA-AgNCs. The obtained $Ag(S_2O_3)_2$@BSA-AgNC fluorescence and particle sizes are pH dependent. For instance, while increase pH of $Ag(S_2O_3)_2$@BSA-AgNCs) without addition of analyte which enhance the fluorescence intensity of AgNCs and subsequently particle size was decreased. The addition of Hg^{2+} to the probe solution fluorescence intensity was quenched at 548 nm with an excitation wavelength of 462 nm. Further, a good linearity was observed from 4 to 400 nM. This methodology was applied to the detection of Hg^{2+} in tap, lake, and river water samples. The thiosulfate presence in AgNCs induced the sensitivity and reached the detection limit level of 4 nM.

The AgNCs are also widely used as probes for the detection of toxic and biochemicals, because of their simple synthesis and cost-effectiveness. Sung and co-workers have employed the detection and also removal of Hg^{2+} from environmental samples using highly fluorescent DHLA-AgNCs with the size of 2 nm [55]. DHLA-AgNCs show an emission maximum at 671 nm upon the excitation wavelength at 430 nm. A quantum yield obtained for DHLA-AgNCs is 3.3%. Once again, the addition of Hg^{2+} produced a quenching of the fluorescence intensity which attributed to aggregation of DHLA-AgNCs, and it was confirmed by TEM. Further, a very low detection limit of 2.8 nM was obtained for DHLA-AgNCs, and this methodology has been applied to the determination as well as removal of Hg^{2+} in different environmental water samples.

The DNA-capped NCs are promising materials and have exposed a high sensitivity and selectivity for the detection of Hg^{2+}. Generally, the helical structures are used to bind Hg^{2+} into DNA, and the metal core also has the strong affinity with Hg^{2+}. For example, DNA with guanine-rich ss (single stranded) and ds (double stranded) have been used for the synthesis of AgNCs [56]. The ds-DNA-AuNCs showed higher fluorescence and better stability than ss-DNA-AuNCs. Thus, ds-DNA-AuNCs were employed for the detection of Hg^{2+} and Cu^{2+}. In this work, EDTA (ethylenediaminetetraacetic acid) was used as masking agent of Cu^{2+} for the selective detection of Hg^{2+}. Good linearity was observed in the range 6–160 nM and 6–240 nM, and detection limits of 2.1 and 3.4 nM were obtained for Hg^{2+} and Cu^{2+}, respectively. To demonstrate the practical applicability, this method was successfully applied for the detection of Hg^{2+} and Cu^{2+} in river water samples.

One pot simple reduction method was used to synthesize carboxyfluorescein (FAM)-labeled DNA-capped AgNCs (DNA-AgNCs) [57]. This nanoprobe shows an emission signal at 625 nm while excited at 562, respectively, and is successfully used them for the quantification of Hg^{2+} and Cu^{2+} based on decreasing fluorescence red emission at 625 nm as a result of quenching. The obtained stability constant of EDTA with Hg^{2+} (21.5) was slightly higher than that with Cu^{2+} (18.8), and it indicates that the Cu^{2+}-EDTA complex is more stable than the Cu^{2+}-AgNC complex. Further, the Hg^{2+}-AgNC complex is more stable than Cu^{2+}-AgNC complex, and therefore the high affinity of EDTA with Cu^{2+} gives the advantage to chelate Cu^{2+} and selectively detect the Hg^{2+}. Further, low detection limits of 1.03 and 2.77 nM for Hg^{2+} and Cu^{2+}, respectively, were obtained, and also this probe was applied for the determination of these ions in tap water samples. In another report, DNA (5′-CCC ACC CAC CCA CCC GGG TCA TCA AGA TAC AGC AAG AAG-3′)-capped AgNCs (DNA-AgNCs) with an average size of 1.5 nm show the emission maximum at 768 nm (λ_{ex}, 717 nm), and the quantum yield was calculated to be 5% [58]. After the addition of Hg^{2+}, the fluorescence of DNA-AgNCs was quenched. The good linearity was observed from 1.9 to 24 nM and the detection limit was found to be 1.9 nM. Finally, this system was applied for the detection of spiked Hg^{2+} in tap water samples. Further, a higher sensitivity for Hg^{2+} has been achieved using a label-free hairpin DNA-scaffolded AgNC [59]. It shows an emission wavelength of 576 nm while it was excited at 490 nm. The fluorescence detection of Hg^{2+} was performed by coupling of hairpin

DNA-scaffolded AgNCs with exonuclease III in order to get an assisted target recycling amplification. With this strategy, the detection limit was as low as 24 pM. Moreover, the low-cost fluorescent sensing system exhibited high reproducibility and specificity, thus representing an optimal sensing platform for rapid screening of Hg^{2+} in environmental water samples. Among the different nanoprobes for the detection of Hg^{2+}, DNA-labeled Au or AgNCs have shown more selectivity and sensitivity. For example, label-free hairpin DNA-scaffolded AgNCs have shown picomolar-level detection limit with high selectivity. The obtained high selectivity and sensitivity are due to the design of DNA and their helical structures [59].

Recently, fluorescent bimetallic nanoparticles have received great attention because of their dual fluorescent properties. A highly sensitive Hg^{2+} sensor was fabricated with lysozyme-capped Ag/AuNCs by T.H. Chen et al. [36]. The lysozyme-capped Ag/AuNCs (Lys-Ag/AuNCs) exhibit two emission maxima at 417 and 613 nm upon excitation at 400 nm. It is suspected to be the obtained two emissions are due to the presence of two different sized NCs. Addition of Hg^{2+} to Lys-Ag/AuNCs gave rise to decrease fluorescence at 417 and 613 nm, and the detection limit was estimated to be 1 nM by ratiometric fluorescence method. The obtained high sensitivity is due to the sensitive metallophilic interaction of Au^{+} and Hg^{2+}. Further, the Ag effect of Lys-Ag/AuNCs, because Hg^{2+} can also have a metallophilic interaction with Ag^{+} as similar as Au^{+}. Once again, this method was applied to the detection of Hg^{2+} in tap water samples.

Further, the nanoclusters are also used for the determination of another dangerous heavy metal Pb^{2+}. It has been found that lead poisoning mainly affects the brain of the human body. The usual symptoms may include memory problems, abdominal pain, constipation, headaches, inability to have children, and tingling in the hands and feet. The Pb^{2+} was quantified by BSA-Ag@AuNCs based on the suppression of the surface energy transfer between acridine orange and gold nanoparticles [60]. The emission of fluorescence at 620 nm was observed when the excitation was performed at 500 nm. Further, the observed emission at 620 nm was quenched upon addition of Pb^{2+}. The sensing mechanism of Pb^{2+} is a metallophilic interaction-based aggregation-induced fluorescence quenching. It was noted that the initial BSA-Ag@AuNC particle size of 1.5 nm increased to 2.5 nm after addition of Pb^{2+} as a result of aggregation. The particle aggregation is due to the binding of Pb^{2+} with BSA. Generally, Pb^{2+} can bind with BSA through their carboxylate functional groups of amino acids, and it led to the particle aggregations. Using this approach, a detection limit of 2 nM Pb^{2+} was obtained, and this probe was utilized for the detection of Pb^{2+} in drinking water samples.

Further, Zhiqin et al. reported the detection of Pb^{2+} by using GSH and 11-MUA functionalized AuNDs (GSH@MUA-AuNDs) [61]. First nonfluorescent THPC/GSH dual ligand-stabilized AuNPs were synthesized by etching, and then dual ligands were exchanged with MUA to obtain a highly fluorescent nanoprobe. The resultant gold nanodots have shown a green emission under UV light at 507 nm upon applying the excitation at 377 nm as depicted in Fig. 9.2a, d. TEM images exhibit that the average diameter of GSH@MUA-AuNDs is 1.7 ± 0.2 nm (Fig. 9.2b, c). It was apparent that fluorescence was quenched upon increasing

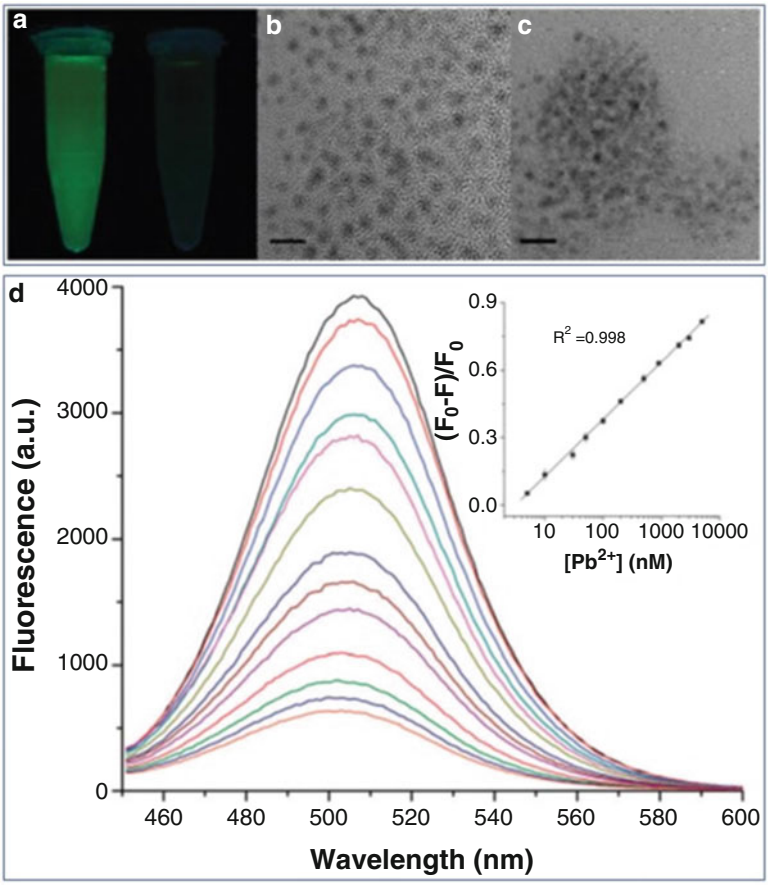

Fig. 9.2 (**a**) Photographs of the AuNDs in the absence (*left*) and presence (*right*) of Pb^{2+} under 365 nm UV lamp illumination. (**b**, **c**) are the corresponding HR-TEM images of the AuNDs in the absence and presence of Pb^{2+}, respectively. Scale bar = 5 nm. (**d**) Fluorescence emission spectra of AuNDs in deionized water in the presence of 0, 5, 10, 30, 50, 100, 200, 500, 900, 2000, 3000, 4000, and 5000 nM of Pb^{2+}. *Inset*: plot of the relative fluorescence reduction versus the Pb^{2+} concentration (Reprinted by permission from The Royal Society of Chemistry: [Chemical Communications] 47, 11,981–11,983, Copyright 2011)

concentration of Pb^{2+}, and good linearity was observed from 5 nM to 5 μM with a detection limit of 2 nM. A correlation coefficient (R^2) was calculated to be 0.998 (inset of Fig. 9.2d). No surprise, again the fluorescence quenching was attributed to the aggregation of GSH@MUA-AuNDs due to the coordination of —COOH with Pb^{2+}. This methodology was applied to the detection of Pb^{2+} in lake water samples.

Copper is one of the heavy metals. Copper toxicity is known as copperiedus and refers to the concerns of an excess of copper in the human body. The fluorescent nanoclusters are also used for the determination of Cu^{2+} as it was found that

chronic exposure to copper can cause kidney and liver diseases as mentioned earlier. Recently, Ma et al. reported that amino acid staining diazo dye, namely, amido black 10B, is used to synthesize AgNCs with size of 1.3 nm [62]. Firstly, $AgNO_3$ solution was heated to 60 °C with constant stirring, and then $NaBH_4$ was added to reduce the silver ions. Finally, the addition of amido black 10B produced the blue emittive AgNCs. The synthesized amido black 10B-capped Ag nanocluster (AB-AgNCs) exhibited a strong and stable blue fluorescence emission at 420 nm for applying an excitation at 315 nm. The fluorescence of AB-AgNCs was quenched when Cu^{2+} was added to the medium due to aggregation as a result of strong interaction between Cu^{2+} and the azo and hydroxyl groups of AB on the surface of AgNCs. Further, TEM was used to detect the size of the nanocluster before and after addition of Cu^{2+} and found that the size was increased from 1.3 nm to 5.25 nm. The azo and hydroxyl functional groups of AB 10B promote to achieve the higher detection limit (4 nM) toward Cu^{2+}. The bimetallic NC-based Cu^{2+} also was demonstrated. A rapid and simple microwave irradiation method was used to fabricate the bimetallic GSH-Ag@AuNCs [63]. The bimetallic nanocluster shows a higher quantum yield (7.8%) compared with the monometallic AuNCs (2.2%). Further, the systematic variation of metal molar ratio (Ag/Au) was investigated and found that the emission intensity was increased up to 0.1 and 0.2 molar and after that declined and also noted that emission wavelength was shifted from 610 to 618 nm. Further, the fluorescence intensity was quenched after addition of Cu^{2+}, S^{2-}, I^{-}, cysteine, and GSH, and the detection limits were found to be 2, 5, 5, 10, and 9 nM, respectively. The sensing mechanism was proposed based on the obtained fluorescence and life time results of GSH-Ag@AuNCs. The obtained fluorescence quenching of GSH-Ag@AuNCs in the presence of Cu^{2+}, S^{2-}, I^{-}, cysteine, and GSH is suspected to be the interaction with Ag^{+} present in GSH-Ag@AuNCs. As a result the formation of insoluble silver salt on the surface of NCs or may be the detachment of Ag^{+} from NCs.

A routine wet chemical method was used to synthesize water-soluble gold nanoclusters with methionine as stabilizing and also reducing agent (Mt-AuNCs) [64]. It has been reported that Mt-AuNCs are highly stable toward different pH and temperature. Briefly, methionine and $HAuCl_4$ are mixed, and a NaOH solution was added with constant stirring and was incubated 37 °C for 6 h. Met-AuNCs present excitation and emission wavelengths at 330 and 520 nm, respectively. The obtained particles size are 2.5 nm with a quantum yield of 2.8%. After the addition of Cu^{2+}, the fluorescence intensity was quenched, and good linearity was observed from 50 nM to 8 μM and the detection limit was found to be 7.9 nM. The obtained high selectivity is due to the strong coordination of Cu^{2+} with methionine, and it inhibited the ligand to metal charge transfer. As a result, the fluorescence of AuNCs was quenched. EDTA chelator was used for binding competition of Met-AuNCs with Cu^{2+}. The quenching fluorescence of Met-AuNCs, after the addition of Cu^{2+}, was restored (almost 94%), while EDTA was introduced. These results confirmed that the interaction of Met-AuNCs with Cu^{2+} was indeed through the coordination. Finally, soil and different environmental samples were evaluated to detect Cu^{2+} using this methodology. Further, human hemoglobin-capped AuNCs (HH-AuNCs) also were applied for the detection of Cu^{2+} and histidine [65]. These NCs exhibit an emission maximum at 450 nm, when they are excited at 365 nm. The HH-AuNCs

act as dual sensor for the determination of Cu^{2+} and also one of the important amino acid of histidine. It has been reported that the fluorescence of AuNCs was quenched after addition of Cu^{2+} due to the aggregation of HH-AuNCs. Surprisingly, a reversible fluorescence recovery was observed while adding the histidine into the HH-AuNCs/Cu^{2+} aggregate. The observed de-aggregation is due to the His-Cu^{2+} complex formation. The fluorescence quenching and enhancement were observed during the addition of Cu^{2+} and histidine in the range of 0.1–20 μM and 1–21 μM, respectively. Moreover, the HH-AuNCs show the detection limits of 28 nM and 0.6 μM for Cu^{2+} and histidine, respectively. For the practical application, these two analyte determinations were demonstrated in human serum and also environmental water samples. Among the different nanoclusters, amido black 10B-capped AgNCs are interesting nanomaterials to detect Cu^{2+} with very high sensitivity [62]. The bimetallic nanomaterials (GSH-Ag@AuNCs) also have shown the high selectivity and sensitivity for the detection of Cu^{2+}, because of dual emissive nature and bimetallic nature [63].

Silver is naturally an abundant heavy metal and widely used by people to make jewelry, electronic equipment, silverware, dental filling, etc. Silver could be found at hazardous waste sites in the form of these compounds mixed with soil and/or water. Therefore, these silver compounds will be the main topic of this profile. Throughout the profile, the various silver compounds will at times be referred to simply as silver. Further, the nanoclusters were used to detect the Ag^{+} as it considered one of the pollutants for the environment. It was found that chronic exposure of Ag^{+} can cause some health effects including cytotoxicity, organ failure, and reduction in mitochondrial function. A rapid and sensitive detection of Ag^{+} was achieved with bovine serum albumin-stabilized gold nanoclusters (BSA-AuNCs) [66]. The synthesized BSA-AuNCs are capable to perform the peroxidase-like activity which can catalytically oxidize the 3,3′,5,5′-tetramethylbenzidine (TMB) by H_2O_2. Peroxidase-like activity can be inhibited by Ag^{+} owing to its strong interaction with nanoclusters of Au° through a redox reaction. The high specificity of the Ag-Au interaction provides excellent selectivity over potential interfering metal ions. The lowest detection of Ag^{+} was found to be 0.204 μM, and this method was applied to detect Ag^{+} in lake water samples.

In another report, Ag^{+} ion was determined directly by BSA-AuNCs. BSA-AuNCs was synthesized by microwave-assisted method [67]. BSA-AuNCs show an emission maximum around 600 nm upon excitation at 350 nm. Fig. 9.3 depicted that while increasing Ag^{+} ion concentration, the fluorescence was enhanced together with a blueshift of the fluorescence maximum. Significantly the red color of BSA-AuNCs changed to orange (inset in Fig. 9.3b). The fluorescence intensity ratio was linearly increased upon the addition of Ag^{+} (Fig. 9.3b). The color and fluorescent spectral changes under UV light were ascribed to the formation of hybrid Ag@AuNCs. Then, based on the emission enhancement, the concentration of Ag^{+} was determined. The good linearity was observed from 0 to 20 μM, and the detection limit was found to be 0.1 μM.

Maria et al. reported the GSH-stabilized AuNCs, and it shows an emission wavelength at 611 nm for the excitation at 396 nm. Such NCs were used to investigate

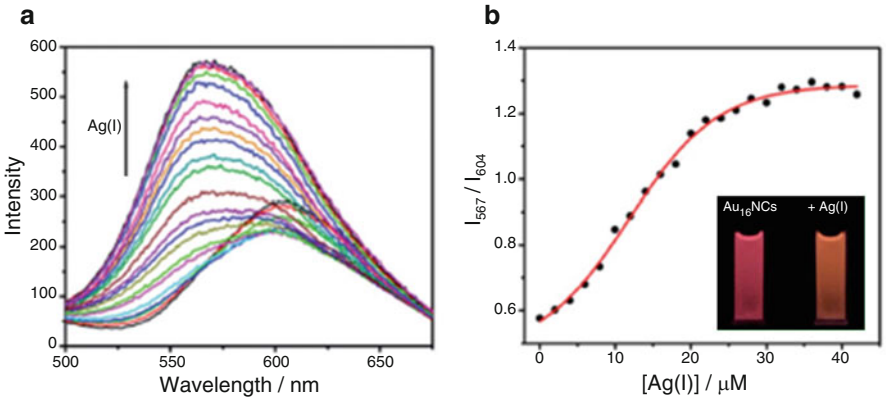

Fig. 9.3 (**a**) Fluorescence spectra of BSA@AuNCs (1 mg/mL) in buffer solution (pH 7.5) measured 20 min after the addition of different amounts of $AgNO_3$ (0–40.0 mM; λ_{ex}, 350 nm), and (**b**) the fluorescence intensity ratio changes upon the addition of different amounts of $AgNO_3$. *Inset of* ***b***: The fluorescence color changes with addition of Ag^+ under ultraviolet light (Reprinted by permission from The Royal Society of Chemistry: [Nanoscale] 4, 2251–2254. Copyright 2012)

the fluorescence effect of GSH-AuNCs with Na^+ and K^+ ion concentrations from 0.1 to 1 mM. A fluorescence intensity enhancement was observed after the addition of these ions. It is expected that Na^+ and K^+ ions can bind with GSH and form a complex. Because of the week stabilization of NCs, it can induce the aggregation of AuNCs through the inter cluster interaction ($Au^+ \ldots\ldots\ldots Au^+$). Due to the aggregation of NCs, the fluorescence was enhanced. Moreover, KSCN addition also gave rise to a large fluorescence enhancement of GSH-AuNCs. This fact was attributed to a decrease in the bandgap of AuNCs that was calculated using the Kubelka-Munk equation, and values from 2.80 eV to 1.42 eV were obtained after the addition of KSCN and Na_2SO_3. Further, KSCN received a special attention; the fluorescence effect of GSH-AuNCs in the presence of KSCN was monitored at pH 4.0. The obtained fluorescence enhancement was due to the ligand exchange mechanism. It is expected that the AuNC ligand GSH could liberate and SCN^- could bind with AuNCs [68].

Iron is considered an important metal, and it's one of the main cofactors in many proteins and involves various biological activities which include oxygen transport, DNA synthesis, and energy metabolism [69]. On the other hand, the excess of iron intake may give a clue to potential toxicity. Therefore, the determination of ferrous or ferric form (Fe^{2+}or Fe^{3+}) of iron is very significant for biomedical application. The indirect method was applied for Fe^{2+} quantification by BSA-AuNCs probe. It has been reported that fluorescence of BSA-AuNCs was quenched by hydroxyl radical that are produced by Fenton reaction between Fe^{2+} and H_2O_2 [70]. Thus, the determination of Fe^{2+} was carried out by fluorescence quenching as a result with the amount of OH^- generated from "Fenton reaction." A good linearity was observed from 0.08 to 100 μM of Fe^{2+} with a detection limit of 24 nM. Moreover, this method

has been applied to the detection of Fe^{2+} from cerebrospinal fluids of rat as part of Alzheimer disease treatment [71]. In another report, ferric form (Fe^{3+}) of iron was detected by using AuNCs. To construct the probe, L-proline-stabilized AuNCs were synthesized by wet chemical method and exhibit the blue emission under UV light at 440 nm while excited at 360 nm. A quenching of the fluorescence was observed when the concentration of Fe^{3+} increased due to an aggregation of the L-proline-AuNCs. This methodology gave rise to a good linear response from 5 to 2000 μM with a detection limit was found to be 2 μM. The present probe was successfully applied to the determination of Fe^{3+} in serum samples [72]. Similarly, L-DOPA-AuNCs also were used for the detection of Fe^{3+} following a similar scheme of aggregation upon addition of Fe^{3+}, producing a decrease of the fluorescence at 525 nm using an excitation source at 360 nm. Good linearity was observed from 5 to 1280 μM, with a detection limit of 3.5 μM, and these probes were evaluated for the detection of Fe^{3+} in tap, lake water and iron supplement tablets [73].

Among the heavy metals, Arsenic is considered to be one of the dangerous pollutants to the environment and living beings. The arsenic in water mainly exhibited in two forms such as trivalent arsenite and pentavalent arsenate. It was found that arsenite is significantly more toxic to humans than arsenate due to its high affinity for sulfhydryl groups of proteins and dithiols such as glutaredoxin which may disrupt intracellular oxidation-reduction homeostasis. Therefore, the determination of arsenic is imperative. Recently, Banerjee and co-workers have fabricated the fluorescent nanoprobe for the quantification of arsenite (As^{3+}) [74]. Fluorescent AuNCs were synthesized by core etching method by using dipeptide L-cysteinyl-L-cysteine (Cy-Cy) with average size of 1.5 nm. These Cy-Cy-AuNCs exhibit luminescence at 410 nm when they are excited at 300 nm and obtained a very high QY of 41.3%. As prepared, Cy-Cy-AuNCs were used as probe for the detection of As^{3+}, without further any modification. An enhancement of the fluorescence was observed upon addition of As^{3+} to the Cy-Cy-AuNC solution. It is expected the strong interaction of As^{3+} with the thiolated groups of Cy-Cy-AuNCs. Further, a high sensitivity was achieved and it shows a detection limit of 53.7 nM. Further, succinic acid was used to examine the reusable property of Cy-Cy-AuNCs for the detection of As^{3+}. It is known that carboxyl group of succinic acid can chelate with As^{3+}. The addition of succinic acid into Cy-Cy-AuNCs did not affect the fluorescence of Cy-Cy-AuNCs. For the addition of succinic acid into Cy-Cy-AuNCs in the presence of As^{3+}, the fluorescence was quenched. Because of the removal of As^{3+} from Cy-Cy-AuNCs and chelate with succinic acid. These results are confirmed that the Cy-Cy-AuNC probe could be reusable for the detection of As^{3+}.

Another important toxic metal is chromium, and it exists in the environment with two forms such as Cr^{3+} and Cr^{6+}. Chromium is responsible for severe environmental pollution and toxic to the living beings. Hence, sensing chromium is a great interest for analytical chemist. In 2013, Jian et al. have developed the probe 11-MUA-AuNCs for the detection of Cr^{3+} and Cr^{6+}. The 11-MUA-AuNCs exhibit a unique fluorescence excitation at 285 nm, with a maximum emission observed

at 608 nm, and a QY of 2.4%. A fluorescence quenching was observed upon the addition of Cr^{3+} due to the binding of Cr^{3+} with 11-MUA-AuNCs. For selectivity study, 10 mM of different metal ions were examined (Li^{+}, Na^{+}, K^{+}, Al^{3+}, Mg^{2+}, Mn^{2+}, Ca^{2+}, Fe^{2+}, Fe^{3+}, Ni^{2+}, Cu^{2+}, Co^{2+}, Zn^{2+}, Hg^{2+}, Cd^{2+}, Pb^{2+}, and Ag^{+}), in HEPES buffer. The fluorescence 11-MUA-AuNCs did not quench after the addition of different metal ions, excluding Cd^{2+}, Fe^{3+}, Pb^{2+}, Hg^{2+}, and Cu^{2+}. To further improve the selectivity of 11-MUA-AuNCs for the detection of Cr^{3+}, EDTA was used as a masking agent to chelate the interfering ions of Cd^{2+}, Fe^{3+}, Pb^{2+}, Hg^{2+}, and Cu^{2+}. As a result, there are no obvious changes in the fluorescence of 11-MUA-AuNCs even in the presence of Cd^{2+}, Fe^{3+}, Pb^{2+}, Hg^{2+}, and Cu^{2+} along with other common metal ions. Based on the fluorescence quenching, the detection limit was found to be 26 nM. Additionally, these NCs also were employed to detect Cr^{6+}, using ascorbic acid as mild reducing agent to convert Cr^{6+} into Cr^{3+} [75].

On the other hand, anion sensors are also important. For example, cyanide, sulfide, chloride, iodide, nitride, and fluoride are highly toxic anions present in contaminated water. These anions are responsible for water pollution and acid rain. Hence, the detection of anions is an essential. The dual metal NCs of BSA-Ce@AuNCs (containing 22 Au and 8 Ce atoms) have developed for the detection of cyanide. It displayed red emission under a UV light source, and two intensity maxima were observed at 410 and 658 nm (dual emission) when using an excitation wavelength of 325 nm. These NCs were evaluated as probe for the detection of cyanide in drinking water. In this work, the addition of cyanide generated a fluorescence quenching at 658 nm, whereas the fluorescence was enhanced at 410 nm. The etching of Au core by CN^{-} quenched the fluorescence at 658 nm, whereas the formation of $[Au(CN)_2]^{-}$ enhanced the fluorescence at 410 nm. Cyanide detection was performed at pH 12, with a linear response from 0.1 to 15 μM and a detection limit of 50 nM. This methodology was applied for the detection of cyanide in drinking and pond water samples [76].

Very recently, Vasimalai et al. reported a CN^{-} sensing probe using PEG-coated trithiocyanuric acid AuNDs (TCA-AuNDs) with 3.3 nm particle size. This is the first report for the synthesis of red emittive AuNDs that is performed within 10 min at room temperature. TCA-AuNDs were prepared by adding gold chloride solution into green emittive TCA with constant stirring, and then pH of the solution was changed to basic. Subsequently, PEG was added; after 10 min of stirring, the red emittive TCA-AuNDs were formed. The UV-vis spectral changes of TCA-AuNDs were observed upon the addition of μM concentration of CN^{-} (Fig. 9.4a). Moreover, TCA-AuNDs exhibit an emission maximum at 623 nm upon excitation at 410 nm and a QY of ∼10%. Addition of CN^{-} produces a decrease of the fluorescence of TCA-AuNDs, obtaining a linear response from 0.29 to 8.87 μM (Fig. 9.4b) and a detection limit of 150 nM. These probes are highly selective even in the presence of 1000 μM concentration of common interferences present in water samples, with the exception of Pb^{2+}, Cd^{2+}, and Hg^{2+}, although the use of glutathione and BSA as masking agents drastically minimized the interference effect. The fluorescence quenching is due to the formation of $[Au(CN)_2]^{-}$ complex and liberation of TCA from AuNDs, experiments confirmed by mass spectrometry

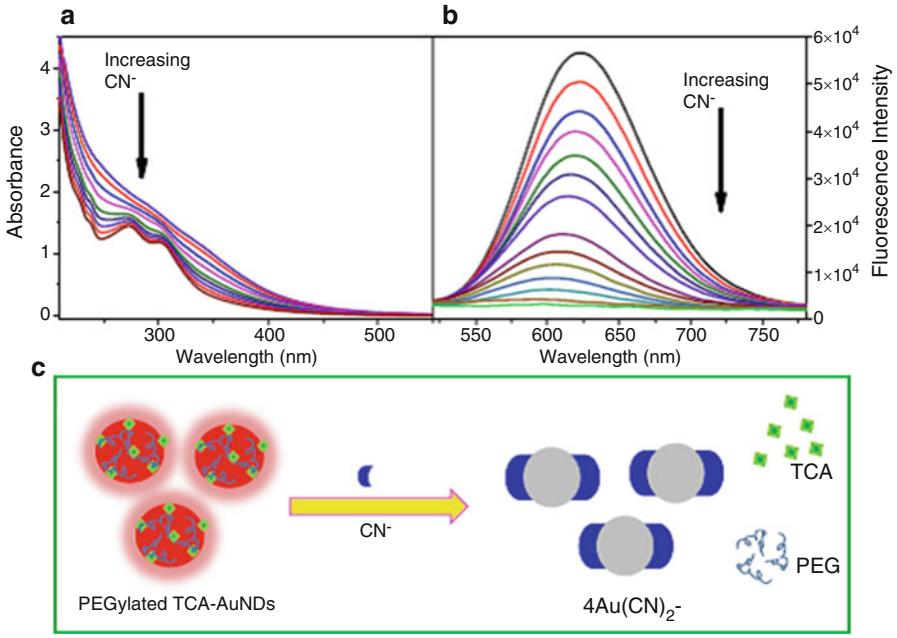

Fig. 9.4 (**a**) UV-vis spectra of TCA-AuNDs with an increasing μM concentration of CN^- ions. (**b**) Fluorescence spectra of TCA-AuNDs with an increasing μM concentration of CN^- ions (λ_{ex}, 410 nm; λ_{em}, 623 nm) and (**c**) schematic representation for the mechanism elucidation of the interaction of cyanide with TCA-AuNDs

(Fig. 9.4c). These TCA-AuNDs have been successfully evaluated as highly sensitive and selective probe for cyanide determination in environmental water samples, including tap, river, lake, and sea water [77].

Furthermore, nanoclusters have been utilized to detect the sulfide ions (S^{2-}) which are also considered as very drastic pollutants to the environment. Haiyun et al. reported the red emittive lysozyme-capped silver NCs (Lys-AgNCs) as probe for sensing of sulfide ions. Lys-AgNCs emit fluorescence at 606 nm upon excitation at 453 nm. After the addition of S^{2-}, the fluorescence was quenched, and a good linear response from 5 μM to 100 μM was observed with a detection limit of 1.1 μM. The formation of Ag_2S is caused by the aggregation and decrease of the luminescence, and this method was successfully applied to the determination of S^{2-} in tap water [78]. Another group has developed the probe of papain-AuNCs for the sensing of S^{2-}. In this work, the emission of papain-AuNCs (excitation and emission wavelengths of 470 and 650 nm, respectively) was quenched in the presence of sulfide ions due to the formation of Au_2S. A linear range for the detection of S^{2-} was observed from 0.5 to 80 mM, and the detection limit obtained was 380 μM for the detection of this ion in different environmental water samples [79].

The detection of oxidative analytes such as nitrite, bromate, and periodate also was performed using BSA-AuNCs with a size of 2 nm. The BSA-AuNCs are showing an emission at 620 nm (excitation wavelength of 365 nm), and a decrease

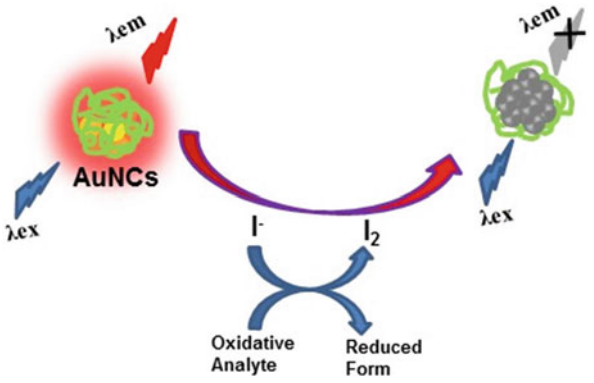

Scheme 9.2 Schematic illustration of iodide detection by using BSA-AuNCs

of emission intensity was observed against increasing concentration of all these ions. This is a simple experimental setup for non-titrimetric determination of nitrite, bromate, and periodate. The oxidative species have a capability to oxidize iodide to iodine. The BSA-AuNCs were etched by iodine and excess of iodine. As a result, fluorescence quenching was observed. Based on fluorescence quenching, the detection limits were calculated to be of 11.7, 1.7, and 1.5 μM for nitrite, bromate, and periodate, respectively [80]. Jilin Yan and co-workers also used the same BSA-AuNCs for the detection of iodide [81]. The presence of iodide produced an oxidation of the metal core owing to an etching process as illustrated in Scheme 9.2. While adding the excess of iodine into the medium, iodine became iodide, and then it acts as a strong etching agent to dissolve gold as shown below (Eqs. 1–3). Further, the fluorescence was quenched upon increasing concentration of analyte into the BSA-AuNCs. Based on this principle, I^- can be determined and observed a linear response from 10 nM to 1 μM with a detection limit of 2.8 nM. Tap and pond water samples are used to demonstrate the practical application of this method:

$$2Au_{(S)} + I^- + I_3^- \rightarrow 2AuI_2^- \tag{9.1}$$

$$Au\,(I) + I^- + I_3^- \rightarrow AuI_4^- \tag{9.2}$$

$$2AuI_2^- + 2I_3^- \rightarrow 2AuI_4^- + 2I^- \tag{9.3}$$

In another report, PEI-AgNCs were used as probes for the detection of Cl^-, Br^-, and I^-. The PEI-AgNCs show the emission maximum at 455 nm upon excitation at 375 nm. The fluorescence intensity was varied and depended upon the pH of the solution and found that the PEI-AgNCs exhibit a low intensity in lower pH and high intensity in neutral and basic pH. The obtained fluorescence variations are ascribed to the charge distribution at the amine group of PEI. The emission intensity at 455 nm was quenched upon the addition of Cl^- or Br^- or I^-, and

this fluorescence quenching is due to the oxidative-induced aggregation. The PEI-AgNCs are sensitive to detect Cl^-, Br^-, and I^-, because of their lower solubility product constant (Ksp) value of AgCl (1.8×10^{-10}), AgBr (5×10^{-13}), and AgI (8.5×10^{-17}). Good linearity was obtained over the concentration range from 0.5 to 80 μM for Cl^-, 0.1 to 14 μM for Br^-, and 0.05 to 6 μM for I^-, respectively, and the detection limits were found to be 200, 65, and 40 nM for Cl^-, Br^-, and I^-, respectively. This methodology was evaluated in tap and mineral water samples for the detection of Cl^-, Br^-, and I^- [82]. Another one group has developed the nitrite sensing using BSA-AuNC probe [83]. A quenching of the luminescence (375 and 660 nm excitation and emission wavelengths, respectively) was observed in presence of nitrite. It is attributed to the oxidation of Au core of BSA-AuNCs, providing a linear response from 100 nM to 100 μM and a detection limit of 50 nM for the detection of nitrite. In this work, a more complex matrix was evaluated, and detection of nitrite was performed in urine samples [83]. Table 9.2 summarizes the applications of Au and AgNCs for the detection of metal ions, linear range, detection limit, sensing mechanism, and type of sample evaluated (Table 9.2).

Among the several reported methods for the detection of toxic ions, only few methods were achieved for nanomolar level of detection limits [36, 54, 55, 57, 60, 81]. For example, the Lys-Ag/AuNCs (bimetallic NCs) are interesting probes because of their good sensitivity for the detection of Hg^{2+}. The obtained high sensitivity is due to the Ag effect, because Ag core also can bind with the Hg^{2+} similar to Au core. Further, the ratiometric method also gave rise to sensitivity. The fabrication of ligand on NCs also is an important task to achieve good sensitivity and selectivity. The hairpin DNA-scaffolded AgNCs showed the lowest detection limit of 24 pM of Hg^{2+}, and the obtained high sensitivity is due to the strong binding of Hg^{2+} with hairpin DNA [59]. The etching principle strategy is also used to achieve high sensitivity. For example, the oxidation of BSA-AuNC metal core was produced by I^- through the etching process. Based on this principle, I^- was determined and the detection limit was reported to be 2.8 nM [81]. But on the other hand, the selectivity of toxic ion sensors still needs to be developed more. Furthermore, the researchers might apply the detection of toxic ions in other real samples such as cement, paint, food samples, etc.

9.3.2 Detection of Biomolecules

In recent days, the detection of biomolecules has received much attention. The use of luminescent nanomaterials for the detection of biomolecules is a growing trend due to the advantages of high fluorescence, low photobleaching, easy to synthesis, etc. Thus, in this section, we have summarized the most recent applications of luminescent Au and Ag nanoclusters for the detection of biomolecules. Ascorbic acid (AA), dopamine acid (DA), and uric acid (UA) are very essential biomolecules for human health. For example, AA is an essential biomolecule for human beings and its deficiency may lead to scorbutus disease. DA is a neurotransmitter and plays

Table 9.2 Summary of methodologies reported for the detection of metal ions and toxic ions using Au and AgNCs

Analyte	NCs	$\lambda_{ex/em}$	Linear range	LOD	Sensing mechanism	Real sample	References
Hg^{2+}	DNA-AuNCs	N/R	N/R	8.3 nM	Ligand-induced aggregation	Lake water and human urine	[33]
Hg^{2+}	Lys-Ag@AuNCs	417 and 613 nm/400 nm	6–100 nM and 0.8–10 μM	1 nM	Metallophilic interaction	Tap water	[36]
Hg^{2+}	L-Amino acid oxidase-AuNCs	510/630 nm	N/R[a]	50 nM	Metallophilic interaction	Tap and river water	[49]
Hg^{2+}	Threonine@11-MUA-AuNCs	282/606 nm	N/R	0.357 μM	Ligand-induced aggregation	Human serum	[50]
Hg^{2+}	C-Dots@BSA-AuNCs	365/450 and 656 nm	N/R	28 nM	Metallophilic interaction	Mineral, lake, and tap water	[51]
Hg^{2+}	BSA-AuNCs	350/650 nm	N/R	2.98 nM	Metallophilic interaction	N/R	[52]
Hg^{2+}	Peptide-AuNCs	365/650 nm	N/R	7.5 nM	Metallophilic interaction	N/R	[53]
Hg^{2+}	BSA-AgNCs	462/548 nm	4–400 nM	4 nM	Metallophilic interaction	Tap, lake, and river water	[54]
Hg^{2+}	DHLA-AgNCs	430/671 nm	N/R	2.8 nM	Ligand-induced aggregation	Environmental water	[55]
Hg^{2+} and Cu^{2+}	DNA-AgNCs	N/R	6–160 nM and 6–240 nM for Hg^{2+} and Cu^{2+}, respectively	2.1 and 3.4 nM for Hg^{2+} and Cu^{2+}, respectively	Metallophilic interaction	River water	[56]
Hg^{2+} and Cu^{2+}	DNA-AgNCs	562/625 nm	N/R	1.03 and 2.77 nM for Hg^{2+} and Cu^{2+}, respectively	Metallophilic interaction	Tap water	[57]
Hg^{2+}	DNA-AgNCs	717/768 nm	1.9–24 nM	1.9 nM	Metallophilic interaction	Tap water samples	[58]
Hg^{2+}	DNA-AgNCs	490/576 nm	N/R	24 pM	Ligand-induced aggregation	Environmental water	[59]

Pb^{2+}	BSA-Ag@AuNCs	500/620 nm	N/R	2 nM	Ligand-induced aggregation	Drinking water samples	[60]
Pb^{2+}	GSH@MUA-AuNDs	377/507 nm	5 nM–5 μM	2 nM	Ligand-induced aggregation	Lake water sample	[61]
Cu^{2+}	Amido black 10B-AgNCs	315/420 nm	N/R	4 nM	Ligand-induced aggregation	N/R	[62]
Cu^{2+}	GSH-Ag@AuNCs	N/R	N/R	9 nM	Metallophilic interaction	N/R	[63]
Cu^{2+}	Methionine-AuNCs	330/520 nm	50 nM–8 μM	7.9 nM	Ligand-induced aggregation	Environmental samples	[64]
Cu^{2+}	Human hemoglobin-AuNCs	365/450 nm	0.1–20 μM	28 nM	Ligand-induced aggregation	Environmental water	[65]
Ag^{+}	BSA-AuNCs	N/R	N/R	0.204 μM	Interaction with metal core	N/R	[66]
Ag^{+}	BSA-AuNCs	350/600 nm	0–20 μM	0.1 μM	Interaction with Au core	N/R	[67]
Na^{+} and K^{+}	GSH-AuNCs	396/611 nm	0.1–1 mM	N/R	Ligand-induced aggregation	N/R	[68]
Fe^{2+}	BSA-AuNCs	N/R	0.08–2.5 μM and 5.0–100 μM	24 nM	Metallophilic interaction	N/R	[71]
Fe^{3+}	L-Proline-AuNCs	360/440 nm	5–2000 μM	2 μM	Ligand-induced aggregation	Serum samples	[72]
Fe^{3+}	L-DOPA-AuNCs	360/525 nm	5–1280 μM	3.5 μM	Ligand-induced aggregation	Tap water, lake water, and in tablets	[73]
As^{3+}	L-Cysteinyl-L-cysteine-AuNCs	300/410 nm	N/R	53.7 nM	Ligand-induced charge transfer	N/R	[74]

(continued)

Table 9.2 (continued)

Analyte	NCs	$\lambda_{ex/em}$	Linear range	LOD	Sensing mechanism	Real sample	References
Cr^{3+}	11-MUA-AuNCs	285/608 nm	N/R	26 nM	Ligand-induced charge transfer	N/R	[75]
CN^-	BSA-Ce@AuNCs	325/410 and 658 nm	0.1–15 μM	50 nM	Interaction with metal core	Drinking and pond water	[76]
CN^-	TCA-AuNDs	410/623 nm	0.29–8.87 μM	150 nM	Interaction with metal core	Tap, river, lake, and sea water	[77]
S^{2-}	Lys-AgNCs	453/606 nm	5 μM–100 μM	1.1 μM	Interaction with metal core	Tap water	[78]
S^{2-}	Papain-AuNCs	470/650 nm	0.5–80 mM	380 μM	Interaction with metal core	Environmental water	[79]
NO_2^-, Br^-, and IO_4^-	BSA-AuNCs	365/620 nm	N/R	11.7, 1.7, and 1.5 μM for NO_2^-, Br^-, and IO_4^-, respectively	Metallophilic interaction	N/R	[80]
I^-	BSA-AuNCs	370/625 nm	10 nM–1 μM	2.8 nM	Metallophilic interaction	Tap and pond water	[81]
Cl^-, Br^-, and I^-	PEI-AgNCs	375/455 nm	0.5–80 μM for cl^-, 0.1–14 μM for Br^-, and 0.05–6 μM for I^-	200 nM, 65 nM, and 40 nM for cl^-, Br^-, and I^-, respectively	Interaction with Au core	Tap water and mineral water	[82]
NO_2^-	BSA-AuNCs	375/660 nm	100 nM–100 μM	50 nM	Interaction with Au core	Urine	[83]

[a] *N/R* not reported

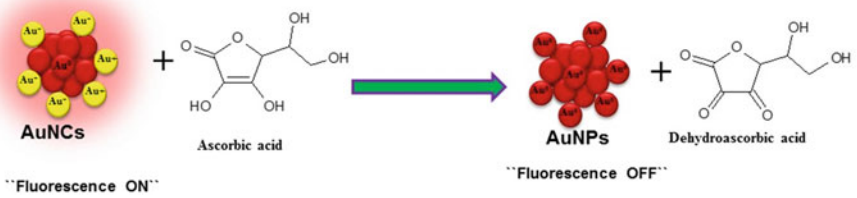

Scheme 9.3 Schematic illustration of the fluorescent sensor of ascorbic acid detection by BSA-AuNCs

an important role in the central nervous system. The DA disequilibrium may cause Parkinson's disease. UA is also another important biomolecule; the deficiency of UA may lead to the disease of hyperuricemia and gout. The sensing of AA, UA, and DA is significant, because of their physiological metabolism process in the human body. In this section, the biomolecule detection can be explained by two categories, such as (i) nonenzymatic detection of biomolecules and (ii) enzymatic detection of biomolecules.

9.3.2.1 Nonenzymatic Detection of Biomolecules

Once again BSA-AuNCs (270 and 620 nm excitation and emission wavelengths, respectively) has been evaluated for the detection of ascorbic acid. In this work, Xianxiang et al. exploited the reducing properties of ascorbic acid in order to modify the oxidation state of the gold present in the AuNCs from Au^{+} to Au^{0} (Scheme 9.3). Thus, the luminescence was quenched in the presence of increasing concentrations of ascorbic acid in plasma samples, obtaining a linear response from 1.5 to 10 nM. The detection limit was found to be 0.2 mM [84].

Folic acid is also an important biomolecule for hematopoietic system. The dearth of folic acid may cause anemia, leucopoenia, etc.; the sensing of folic acid is often important in clinical, pharmaceutical, and food monitoring fields. It has been detected by using BSA-AuNCs. In this work, the BSA-AuNC fluorescence was observed at 652 nm with an excitation wavelength of 505 nm. The fluorescence of BSA-AuNCs was quenched after the addition of CA-AuNPs. Because of the surface plasmon-enhanced energy transfer (SPEET) between CA-AuNPs and BSA-AuNCs [85, 86], the addition of folic acid produced a shift of the absorption of CA-AuNPs from 530 nm to 670 nm, attributed to the aggregation of CA-AuNPs. It was expected that the positively charged AC-AuNPs electrostatically interact with folic acid, and it leads to aggregate of particles. As a result, a recovery of the fluorescence emission of BSA-AuNCs was observed. Based on the fluorescence enhancement occurring as a consequence of the energy transfer, folic acid was determined in tablets and human blood serum samples. Good linear response was observed from 0.11 to 2.27 μM and a detection limit of 0.065 μM [87]. Another approach for the detection of folic acid using BSA-AuNCs was developed by Hongchang et al. The addition of folic acid

gave rise to a quenching of the fluorescence. Then, the presence of overexpressed folate receptor produced a liberation of the folic acid from the BSA-AuNCs (to bind the folate receptor), and the fluorescence was enhanced. Using this approach, a linear range for the detection of folic acid was obtained from 0.27 to 4.5 μM and the detection limit was reported to be 45 nM. Furthermore, the authors used these probes to perform bioimaging studies in tumor cells where the folate receptor was overexpressed [88].

Cysteamine has numerous clinical applications. It has been used as a neuroprotective agent for Parkinson's diseases. The detection of cysteamine was also carried out using BSA-AuNCs as probe. In this case, upon addition of cysteamine, the fluorescence intensity of BSA-AuNCs at 650 nm was quenched. Cysteamine reacts with Au metal core by etching and forms the cysteamine-Au complex. This leads to decrease the fluorescence of BSA-AuNCs. A good linearity was observed from 0.5 to 10 μM and the detection limit was found to be 150 nM. Human serum samples were used to apply this methodology for the detection of cysteamine [89]. Xialzhe et al. have developed the sensing probe of poly(N,N′-methylenebisacrylamide)-capped AuNPs (PDMAM-AuNPs) and BSA-AuNCs for the detection of L-cysteine in urine samples. In this work, the fluorescence intensity of BSA-AuNCs at 620 nm (excitation wavelength at 503 nm) was quenched when they are mixed with PDMAM-AuNPs. The observed fluorescence quenching is due to the Forster resonance energy transfer (FRET) between BSA-AuNCs and PDMAM-AuNPs. Then, addition of L-cysteine forms Au-S bond with PDMAM-AuNPs, and the particle aggregation was obtained. Further, the fluorescence enhancement of BSA-AuNCs was observed, because of the release of BSA-AuNCs from PDMAM-AuNPs. These results confirmed that the addition of L-cysteine defeated the FRET between BSA-AuNCs and PDMAM-AuNPs. This methodology gave rise to a linear range for the detection of L-cysteine from 5 mM to 50 mM and a detection limit of 3.6 μM. Further, this method was validated to determine L-cysteine in human urine sample [90].

Bimetallic BSA-Ag@AuNCs are exhibit an emission maximum at 650 nm (excitation wavelength at 370 nm) with particle size of 2.8 nm. These bimetallic NCs were evaluated as probe for the detection of amino acids such as cysteine and GSH. After the addition of cysteine and GSH, the fluorescence of BSA-Ag@AuNCs was quenched. The obtained fluorescence quenching are ascribed to the formation of nonfluorescent complex via Ag-S bonding. Detection of cysteine can be performed from 20 to 80 nM, with a detection limit of 5.87 nM. A linear response for GSH was observed from 2 to 70 nM, with a detection limit of 1.01 nM. These BSA-Ag@AuNCs were successfully applied to the detection of cysteine and GSH in human plasma samples [91]. Among the different fluorescence nanocluster probes, bi- or multimetallic nanoclusters are effective probe to reach high sensitivity. Because of their multimetallic properties such as dual metal core, dual emission, etc. We hope that this type of multimetallic nanocluster probe will be a spotlight in biosensor research.

GSH detection in Hep G2 cells (human liver cancer cells) was also performed by Shenghao et al., using methionine and MUA dual ligand-functionalized AuNCs (Mt@MUA-AuNCs). These NCs have shown the excitation and emission wave-

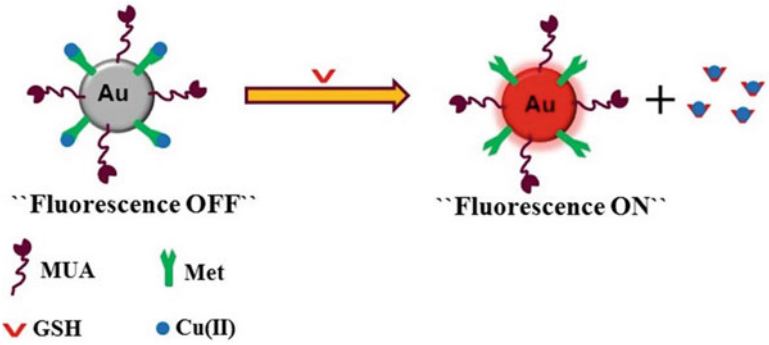

Scheme 9.4 Schematic illustration of fluorescent GSH detection by Mt@MUA-AuNCs

lengths at 275 and 608 nm, respectively, a particle diameter of 1.3 nm, and a high QY of 7.6%. Turn-off and turn-on of the fluorescence were performed by adding Cu^{2+} and GSH, respectively (Scheme 9.4). Based on the fluorescence enhancement, GSH was determined with good linearity from 30 nM to 22.5 μM, and a detection limit of 9.7 nM was obtained [92]. A similar approach was developed by Tian et al., where the fluorescence of BSA-AuNCs (530 and 670 nm excitation and emission wavelengths, respectively) was quenched in the presence of Hg^{2+}, and the addition of GSH generated a fluorescence enhancement attributed to the coordination binding of Hg^{2+} with GSH. Based on this reaction, the concentration of GSH can be determined with a good linear response from 0.04 to 16.0 μM, with a detection limit of 7.0 nM. This methodology was applied to the detection of GSH in living cells and human blood samples [93].

Trypsin is another one biomolecule of interest whose detection has been performed in urine samples using BSA-AuNCs. The addition of trypsin produced the digestion of the BSA on the surface of the NCs, and as a result, the fluorescence of AuNCs was quenched at 650 nm (excitation wavelength of 385 nm). The linearity of this method was observed from 0.01 to 100 μg/mL, with a detection limit for trypsin of 2 ng/mL [94]. Another report described the use of blue and red emittive BSA-AuNCs, synthesized with and without addition of ascorbic acid, respectively. These BSA-AuNCs have a peroxidase-like activity, and the addition of TMB produces a change of the color of the solution to blue. The catalytic activity of BSA-AuNCs decreased in the presence of trypsin, attributed to the cleavage of BSA and aggregation of AuNCs, giving rise to a decrease of the absorbance of TMB at 652 nm, achieving a detection limit of 0.6 μg/mL for the detection of trypsin [95].

Jiang et al. have developed the system for the detection of anticancer drug of mitoxantrone and circulating tumor DNA (ctDNA). The probe of 2-nm-sized GSH-AuNCs with an emission wavelength of 570 nm. Negatively charged GSH-AuNCs interact with positively charged mitoxantrone drug while adding mitoxantrone into GSH-AuNCs. Due to the photoinduced electron transfer from GSH-AuNCs

to mitoxantrone, the fluorescence of GSH-AuNCs was quenched. Addition of ctDNA leads to enhancement of the fluorescence of GSH-AuNCs, because of the conjugation of mitoxantrone drug into double helix structure of ctDNA. Finally, the GSH-AuNCs were freed from the electrostatic binding of mitoxantrone; hence the fluorescence of GSH-AuNCs was enhanced. Based on the fluorescence quenching and enhancement, the mitoxantrone and ctDNA, respectively, were determined. The detection limits of mitoxantrone and ctDNA were determined to be 20 nM and 0.1 μg/mL, respectively. Thus, this approach has been used to perform both ctDNA and drug monitoring [96].

Detection of other biomolecules of interest, such as adenosine-5′-triphosphate (ATP), adenosine, and thrombin, were performed by using red emittive dsDNA-AgNCs with an emission maximum at 635 nm. For this purpose, two tailored DNA sequences, complementary DNA (c-DNA) and signaling probe (s-DNA), were designed. The c-DNA is specially designed with a sequence complementary to aptamer, and the s-DNA contains a link sequence of complementary to c-DNA. The aptamer-associated target c-DNA can bind with s-DNA and form dsDNA and protect the AgNCs. The dsDNA-AgNCs thereafter could close to the guanine-rich sequence, leading to enhanced fluorescence signal readout. The detection limits obtained for ATP, adenosine, and thrombin were 91.6 nM, 103.4 nM, and 8.4 nM, respectively [97]. In another work, Chen and co-workers were used GSH-AuNCs as probe for the detection of ATP and pyrophosphate in human blood plasma samples. First the fluorescence of GSH-AuNCs (excitation and emission wavelengths at 396 and 613 nm, respectively) was quenched by the addition of Fe^{3+}, due to the chelation of GSH-AuNCs-Fe^{3+}, and subsequent recovery of the fluorescence took place after the addition of ATP or pyrophosphate. This is due to the formation of a complex of Fe^{3+} with ATP and pyrophosphate. The methodology gave rise to a linear response from 50 to 500 μM for ATP and from 50 to 100 μM for pyrophosphate. Moreover, the detection limits for ATP and pyrophosphate were found to be ∼43 μM and ∼28 μM, respectively [98]. Dihydronicotinamide adenine dinucleotide (NADH) and nicotinamide adenine dinucleotide (NAD^+) are reduced and oxidized forms of coenzyme, respectively, which are found in all living cells. It contains adenine base and nicotinamide in their structure. In cellular metabolism, this enzyme is involved in redox reactions. Therefore, the monitoring of NADH activity is highly significant for biological studies. In this regard, Siyu et al. reported the use of 1.43 nm trypsin-AgNCs (excitation and emission wavelengths at 580 and 662 nm, respectively) with a QY of 6.2% for the monitoring of NADH activity in biological reactions. The synthesized trypsin-AgNCs have shown the pH-dependent fluorescence. The fluorescence maximum was shifted toward higher wavelength when increasing the pH from 4.5 to 12.5. The fluorescence of trypsin-AgNCs remains unchanged even in the presence of 1000 μmol/L of each K^+, Na^+, Ca^{2+}, Zn^{2+}, Ni^{2+}, Ba^{2+}, Cd^{2+}, Fe^{3+}, Pb^{2+}, Hg^{2+}, Cu^{2+}, glucose, sodium citrate, glutathione, dimethylformamide, acetonitrile, pyridine, benzoic acid, and hydroquinone in phosphate buffer pH 8.2. Whereas in the presence of NADH instead of NAD^+, the fluorescence of trypsin-AgNCs was effectively quenched. Furthermore, ethanol and NAD^+ products are obtained from the oxidation of

NADH. Hence, trypsin-AgNCs were used as probe for ethanol sensing. After the addition of ethanol into a trypsin-AgNC and NAD^+ mixture, the fluorescence was quenched, giving rise to a methodology for detection of ethanol in a range between 10 and 300 μM and with a detection limit of 5 μM [99].

Hemoglobin is the oxygen-containing blood carrier from lungs to the rest of the human body. The lack of hemoglobin can cause anemia, kidney failure, bone marrow problems, etc. Tchang and co-workers developed a methodology based on the use of MUA-AuNDs to carry out the detection of hemoglobin. First, MUA-AuNDs were synthesized from THPC-AuNPs by ligand exchange method. The green emission of the MUA-AuNDs is observed at 520 nm upon excitation at 375 nm. The emission was quenched after addition of hemoglobin due to a redox reaction between MUA-AuNDs and the cofactor of Fe^{2+} present in the hemin units. This probe was shown high selectivity versus different proteins such as serum albumin and carbonic anhydrase. A linear response from 1 to 10 nM and a detection limit of 0.5 nM are achieved for the detection of hemoglobin [100]. Again based on a redox reaction, Chen et al. performed the detection of cholesterol using BSA-AuNCs as a sensing probe. In this work, cholesterol was oxidized by cholesterol oxidase (ChOx) and converted to cholest-4-en-3-one and generating H_2O_2 as by-product. The obtained H_2O_2 degrades the surface of AuNCs, because it acts as an oxidant and it generates disulfide bonds or sulfonates of amino acids present in BSA, destroying the stabilization of AuNCs and thus producing a quenching of the fluorescence, and a detection limit of cholesterol was found to be 12 μM [101].

9.3.2.2 Enzymatic Detection of Biomolecules

In this sense, one of the most common and well-known routes for the synthesis of luminescent AuNCs is based on the use of BSA as stabilizing agent. Thus, many different applications of these AuNCs have been developed so far. BSA-capped nanoclusters are used as probe for several biomolecules owing to the high biocompatibility and also higher stability. Cheng and co-workers have developed a label-free uric acid sensor with BSA-AuNCs. In general, H_2O_2, allantoin, and CO_2 were produced by the reaction of uricase with uric acid as shown in Eq. 4. Then, the hydrogen peroxide acts as a substrate for indirectly detecting the uric acid. As mentioned before, BSA-AuNC was used as sensitive probe for H_2O_2 detection. Thus, the detection of uric acid was performed by analyzing H_2O_2 which was generated by enzymatic reaction between BSA-AuNCs and uricase. A quenching of the emission was observed at 610 nm (excitation wavelength 370 nm). A good linear response was observed from 10 to 800 μM, and a detection limit of 6.6 μM was obtained for H_2O_2. Furthermore, this methodology was applied to the detection of uric acid in complex human serum samples [102].

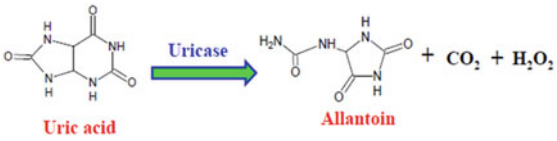

(9.4)

Another report found in the literature is based on a similar principle. In this work, the uric acid was detected directly by using urate oxidase which oxidized the uric acid into allantoin. The fluorescence emission of BSA-AuNCs was quenched after the addition of uric acid, with a linear response from 0.7 to 80 μM and a detection limit of 120 nM. The selectivity of BSA-AuNC probe for the detection of UA was examined with glucose, sucrose, fructose, lactose, urea, glycine, ascorbic acid, and citric acid. The above coexisting chemicals did not interfere for the detection of UA. The obtained specificity is due to the effective catalysis of uricase enzyme to UA [103].

A bit higher emission wavelength (615 nm) was obtained for BSA-AuNCs while excited at 500 nm and used as probe for the detection of dopamine. The red emission of BSA-AuNCs was quenched in the presence of dopamine due to a photoinduced electron transfer process between dopamine and the BSA-AuNCs. Good linearity was observed from 10 nM to 1 μM and a detection limit of 10 nM was reported. Moreover, a visual detection of dopamine also was performed based on the use of peroxidase and 3,3′,5,5′-tetramethylbenzidine (TMB) substrate. This methodology was applied to the detection of dopamine in human serum samples and PC12 cells [104]. Detection of dopamine and tyrosinase was also reported by using GSH-AuNCs. Tyrosinase is a type of polyphenol oxidase that can effectively catalyze the transformation of dopamine to produce o-quinone (Fig. 9.5a), giving rise to a quenching of the luminescence at 610 nm when using an excitation wavelength of 350 nm. Moreover, the polymerization of o-quinone generates a new fluorescence peak around 400 nm. Thus, a fluorescence enhancement can be observed as the concentration of dopamine increases (Fig. 9.5b). This has served as the basis to develop a ratiometric methodology to perform the detection of tyrosinase and dopamine, with detection limits of 0.006 unit mL^{-1} and 1.0 nM, respectively [105].

It is well known that enzymes are involving in different kinds of metabolic processes. Pyrophosphate ion (PPi) plays an important role in several biochemical reactions. Further, PPi is also one of the substrates of alkaline and acid phosphatase (ACP) enzyme. ACP is a digestive enzyme present in mammalian animal tissues and has a role to catalyze the hydrolysis of phosphate esters. Hence, their sensing is essential for biomedical applications. In this case, GSH/MUA-AuNCs were used for the detection of the enzyme acid phosphatase. The GSH/MUA-AuNCs were synthesized through a wet chemical method by simply mixing the reagents in alkaline medium and stirring for 30 min, obtaining orange red emittive AuNCs with an emission maximum at 610 nm (excitation wavelength at 293 nm). First, the fluorescence of GSH/MUA-AuNCs was quenched by the addition of Fe^{3+}, attributed to the binding of Fe^{3+} with MUA or to an electron transfer between AuNCs and Fe^{3+}, giving rise to the aggregation of the nanoclusters. The presence

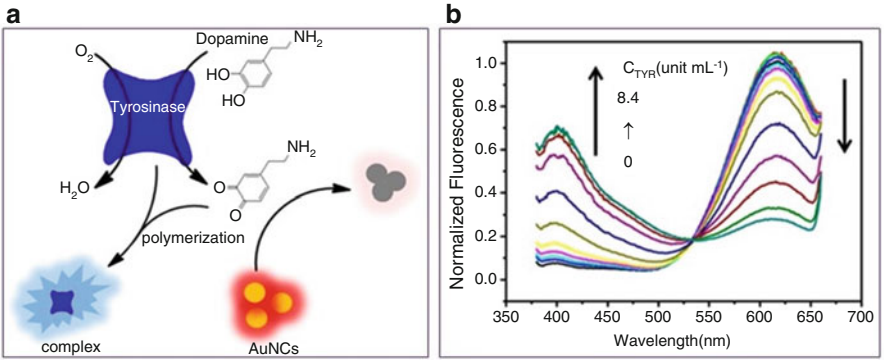

Fig. 9.5 (**a**) Schematic demonstration of the fluorescence method with TYR, DA, and AuNCs. (**b**) Fluorescence spectra of AuNCs with DA and different concentrations of TYR. The concentrations of TYR were 0, 0.006, 0.012, 0.06, 0.12, 0.24, 0.6, 1.2, 2.4, 3.6, 6.0, and 8.4 unit mL^{-1}, respectively (Reprinted by permission from American Chemical Society: [Analytical Chemistry] 87, 4897–4902. Copyright 2015)

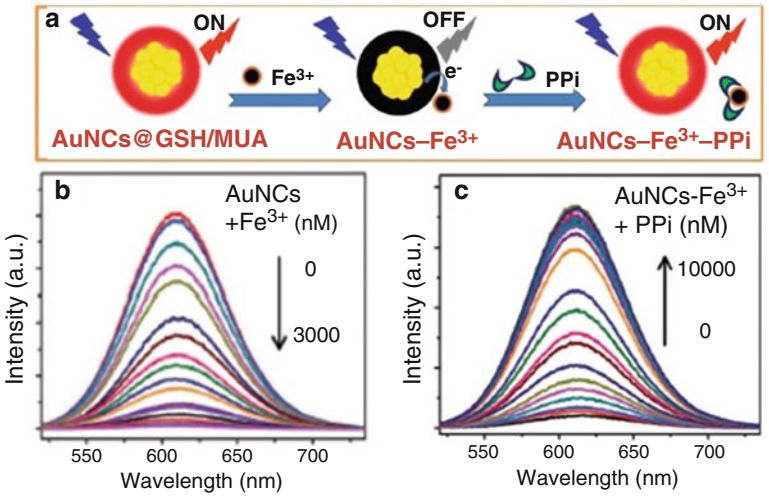

Fig. 9.6 (**a**) Schematic representation of the response mechanism based on the competitive binding of Fe^{3+} between AuNCs@GSH/MUA and PPi. (**b**) The fluorescence response of the AuNCs@GSH/MUA upon addition of different Fe^{3+} concentrations increasing from 0 to 3 μM (*top* to *bottom*) and (**c**) the fluorescence response of the AuNC-Fe^{3+} complexes upon addition of different PPi concentrations increasing from 0 to 10 μM (*bottom* to *top*) (Reprinted by permission from The Royal Society of Chemistry: [Nanoscale] 7, 16,372–16,380. Copyright 2015)

of the enzyme produced a binding of Fe^{3+} with acid phosphatase, generating a recovery of the fluorescence of GSH/MUA-AuNCs (Fig. 9.6), and a detection limit of acid phosphatase was found to be 1 nM [106].

On the other hand, the glucose detection has gained momentum. Glucose is an important source of energy for living beings. The excess of the recommended glucose levels in humans can cause heart diseases, kidney failure, diabetes, etc. [107, 108]. Therefore, the detection of glucose is very important from the public health point of view, and researchers have been focused to develop fast, reliable, sensitive, and selective methods to quantify glucose level that overcome the limitations of the current methods employed in clinical chemistry. For this purpose, the use of AuNCs has been evaluated through different approaches, most of them are based on the quenching of the luminescence of the nanocrystals after oxidation of glucose. Hydrogen peroxide is one of the by-products in the enzymatic reaction from the glucose oxidation in the presence of electron acceptor oxygen as shown in Eq. 5. Thus, most of the methods are developed indirectly to quantify H_2O_2 to monitor the glucose concentration. For instance, apoferritin paired-AuNCs (AP-AuNCs) (455 and 504 nm excitation and emission wavelengths, respectively) efficiently catalyze the oxidation of 3.3′,5.5′-tetramethylbenzidine (TMB) by H_2O_2, producing a blue color. Obviously, TMB acts as mediator to perform the detection of glucose in the presence of glucose oxidase [109]. Lihua et al. used BSA-AuNCs that present peroxidase-like activity, capable of catalyzing the oxidation of glucose by oxygen in the presence of glucose oxidase (GOD) as shown in Eq. 5:

$$\text{Glucose} + O_2 + H_2O + \text{GOD} \rightarrow \text{Gluconic acid} + H_2O_2 \tag{9.5}$$

During the enzymatic reaction, the fluorescence of BSA-AuNCs was quenched, and a linear response is obtained for the detection of glucose from 10 μM to 0.5 mM, with a detection limit of 5 μM [110].

GOD was also used to detect the glucose in urine samples that was based on the use of ovalbumin-AuNCs. The Au-S bond of ovalbumin-AuNCs was destroyed by H_2O_2, which is the by-product of GOD enzymatic reaction. Further, during the GOD enzymatic reaction, the NC surface of Au^+ could be reduced into Au^0, which leads to aggregation of the NCs. The obtained structural deterioration of the ovalbumin-AuNCs leads to quench the fluorescence at 625 nm. A detection limit of 1 μM and a linear response from 5 μM to 10 mM were reported [111]. Xiaodong et al. have synthesized the enzyme-capped nanoclusters. First, THPC-AuNPs, was prepared and used as precursor for synthesizing the enzyme-bound fluorescent AuNCs after etching with thioctic acid functionalized GOD. These GOD-AuNCs show the emission maximum at 650 nm upon excitation at 507 nm and a QY of 7%. These nanoclusters already contain the GOD enzyme on their surface, and oxidize glucose to produce H_2O_2, which leads to quenched the fluorescence of AuNCs. This methodology was applied to the detection of glucose in serum samples, with good linearity from 2.0 to 140 μM and with a detection limit of 0.7 μM [112]. In a similar approach where the enzyme is on the surface of the nanoclusters, horseradish peroxidase-protected AuNCs (HRP-AuNCs) were prepared by a direct synthesis method and used to perform the detection of H_2O_2 from 100 nM to 100 μM with a detection limit of 30 nM [113].

11-MUA-AuNDs are synthesized by ligand exchange method by using THPC-AuNPs as precursors to detect glucose. In this work, the green fluorescence (522 nm) was quenched upon addition of H_2O_2 due to the formation of disulfide products [114]. A wide linear range for detection of H_2O_2 was obtained from 100 nM to 1 mM with a detection limit of 30 nM. Furthermore, 11-MUA-AuNCs were evaluated as probe to detect glucose based on H_2O_2 which is generated by enzymatic catalytic reaction of GOD with glucose. The methodology provided a linear response from 30 mM to 1 mM and a detection limit of 1 mM for detection of glucose in serum samples [115]. It is well known that the tumor cells are in acidic microenvironment due to the high metabolic rates and poor oxygen supply. Hence, the researchers are developing the biomarkers that can sense transition in cellular pH for the early detection of tumors. Red emittive DHLA and γ-cyclodextrin (γ-CD)-capped AuNCs (AuγCD-NCs) were synthesized by Tarasankar et al. and show the pH-dependent fluorescence. The maximum emission was shifted while changing the pH. For instance, at pH 7.7, the maximum emission occurs at 745 nm, whereas a decrease of the pH to 6 produces a redshift of the maximum to 825 nm. This property has been exploited to perform the detection of MCF7 human breast carcinoma cells [116]. BSA-AuNCs coupled with fluorescein isothiocyanate (FITC-BSA-AuNCs) with improved cell permeability and good photostability were used to monitor intracellular pH of Hela cells (Fig. 9.7). The ratiometric pH-sensing probe has shown good linearity in a small pH range from 6.0 to 7.8, although its response is highly selective to changes of the pH even in the presence of several metal ions and amino acids [117].

The same FITC-BSA-AuNCs were used as probe for the detection of H_2O_2, enzymatic activity, and environmental pH monitoring. These NCs have shown dual emission peaks at 525 and 670 nm upon excitation at 488 nm. An effective fluorescence quenching of FITC-BSA-AuNCs was observed upon the addition of H_2O_2, and therefore, enzymatic systems where H_2O_2 is involved, such as glucose oxidase, acetylcholinesterase, and paraoxon, can be also monitored with these probes. The pH also induced a change in the FITC fluorescence, enabling the use of FITC-BSA-AuNCs for the detection of ammonia product-related enzymatic systems. The authors were applied these nanocrystals for the detection of urea in human serum samples by using urease enzyme [118].

Further, Au and AgNCs were used to monitor the enzymatic activities. 1.67-nm-sized peptide-AuNCs (325 and 414 excitation and emission wavelengths, respectively) were applied as probes for protein kinase sensing. The detection was based on the aggregation of phosphorylated peptide-AuNCs triggered by Zr^{4+} coordination, giving rise to a fluorescence quenching that allowed the detection of protein kinase II (CK2) from 0.08 to 2 unit mL^{-1} with a detection limit of 0.027 unit mL^{-1} (Fig. 9.8). The unchanged fluorescent lifetime of AuNCs in the presence of CK2 and ATP with Zr^{4+} confirmed that the present system is a static quenching mechanism. The phosphate groups of peptide-AuNCs can coordinate with Zr^{4+}, which lead to aggregation of the AuNCs. On the other hand, the presence of the kinase inhibitor of ellagic acid produced an enhancement of the fluorescence intensity which was observed allowing also the detection of ellagic acid [119].

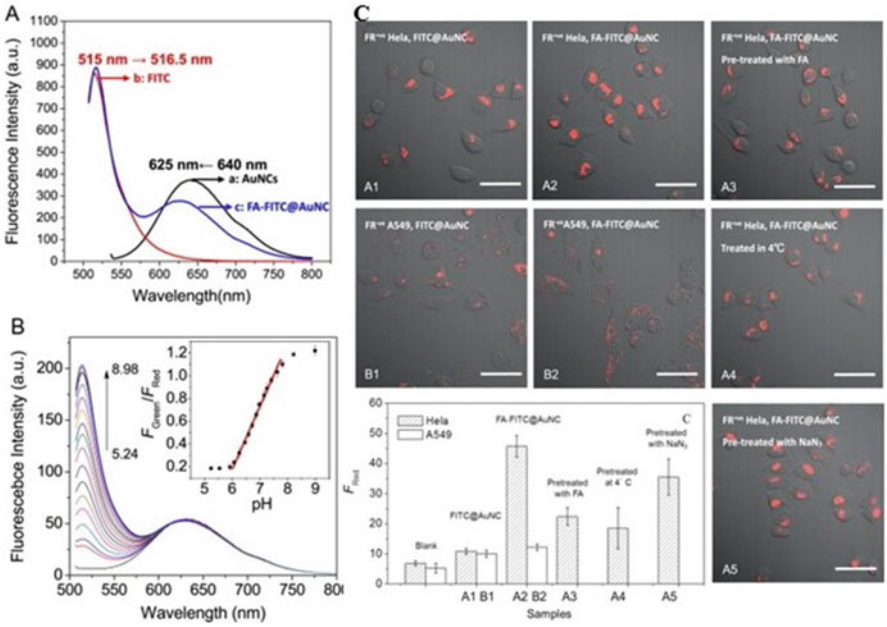

Fig. 9.7 Fluorescent determination of pH. (**a**) Fluorescence spectra of (**a**) AuNCs, (**b**) FITC, and (**c**) FA-FITC@AuNC under 488 nm excitation; (**b**) fluorescence spectra of the ratiometric biosensor to various pH titration. *Inset*: Plot of F_{Green}/F_{Red} as a function of the pH (5.0–9.0) (excited at 488 nm; F_{Green}, 510–550 nm; F_{Red}, 580–680 nm). (**c**) Fluorescent microscopic images showing interaction of FA-FITC@AuNC and FITC@AuNC with (**a**) Hela cells and (**b**) A549 cells: (A1) FR^{+ve} Hela and (B1) FR^{-ve} A549 cells with FITC@AuNC, (A2) FR^{+ve} Hela and (B2) FR^{-ve} A549 with FA-FITC@AuNC of incubation for 2 h at 37 °C, and FR^{+ve} Hela cells incubated with FA-FITC@AuNC for 2 h after treated (A3) with FA for 2 h, (A4) at 4 °C, and (A5) 10 mM NaN3 for 2 h. (**c**) Cellular internalization amount of FA-FITC@AuNC and FITC@AuNC in different types of cell lines under various treatments. Error bar: standard error measurements (SEM). Scale bar, 50 μm (Reprinted by permission from Elsevier: [Biosensors and Bioelectronics], 65, 183–190. Copyright 2015)

GSH-AuNC fluorescence was quenched at 824 nm with an excitation wavelength of 590 nm after the addition of cysteamine-modified gold nanorods (AuNRs) due to a FRET phenomenon between both nanomaterials. Afterward, the fluorescence was turned-on upon addition of glutathione S-transferase (GST). The interaction between GSH and GST is highly specific, and it is stronger than the interaction between the AuNRs and GSH-AuNCs. Hence, the presence of GST produces an increase on the distance between the donor and the acceptor, and the FRET efficiency decreased, giving rise to an increase of the fluorescence of the AuNCs. Based on this principle, the concentration of GST could be determined from 2 to 100 nM, with a detection limit of 1.5 nM [120]. In another report, denatured BSA (dBSA) was prepared by using $NaBH_4$, and afterward it was employed as ligand for the synthesis of fluorescent AuNCs (520 and 640 nm excitation

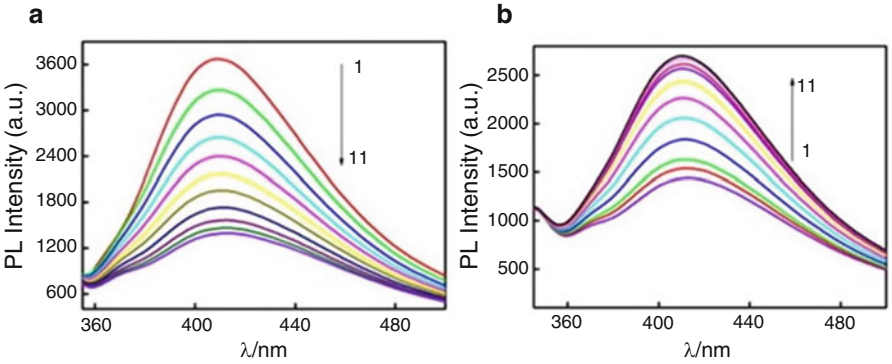

Fig. 9.8 (**a**) PL quenching of the AuNCs treated with various amounts of CK2, followed by the addition of 0.25 mM Zr^{4+}. The concentrations of CK2 were 0, 0.04, 0.08, 0.4, 0.8, 1.0, 1.4, 1.8, 2.0, 4.0, and 8.0 unit mL^{-1} for curves 1–11, respectively. The concentration of ATP was 50 μM. (**b**) PL spectra of the AuNCs in 1% human serum in the presence of 2.0 unit mL^{-1} CK2, 50 μM ATP, and various amounts of ellagic acid, followed by the addition of 0.25 mM Zr^{4+}. The concentrations of ellagic acid were 0, 0.01, 0.02, 0.03, 0.04, 0.05, 0.06, 0.08, 0.1, 0.2, and 0.3 μM for curves 1–11, respectively (Reprinted by permission from Elsevier: [Biosensors and Bioelectronics] 64, 234–240. Copyright 2015)

and emission wavelengths, respectively) which stabilizes the AuNCs due to the presence of 35 cysteine residues that can interact with the surface of AuNCs. dBSA was synthesized by the following steps: Firstly BSA was treated with sodium borohydride by stirring. Then the dBSA was heated for 1 h at 70 °C to remove H_2 gas. Under ambient temperature, $HAuCl_4$ was added into dBSA, followed by 1 M NaOH, and it was allowed to be stirred for 12 h. The obtained dBSA-AuNCs were evaluated as probe for the detection of acetylcholinesterase (AChE) activity. In this methodology, AChE produced the hydrolysis of S-acetylthiocholine iodide (ACTI), generating thiocholine that quenched the emission of the NCs. Thus, the AChE activity was monitored in human serum in a range of concentrations between 0.005 and 0.15 U mL^{-1}, achieving a detection limit of 0.02 mU mL^{-1} [121].

Fluorescent AuNDs-liposome hybrids (11-MUA-AuND/Lip hybrids) were used by H-Tchang and co-workers for the detection of phospholipase C. The fluorescence of 11-MUA-AuND/Lip hybrids (370 and 530 nm excitation and emission wavelengths, respectively) was quenched after vortexing due to the oxidation of the Au-S surface bonds by O_2 molecules. O_2 molecules were permeated into the liposome bilayer of 11-MUA-AuNDs, due to their ultrasmall size, and it leads to quench the fluorescence. In this work, phospholipase C catalyzes the hydrolysis of phosphatidylcholine, inhibiting the quenching of the luminescence, which was used to perform its detection in cancer and normal cells with a detection limit of 0.21 nM [122].

Enhancement of the fluorescence is also the principle for the detection of esterase and alkaline phosphatase (ALP). The presence of both enzymes together with 6-mercaptohexanol and TCHP-AuNPs gave rise to the generation of green

fluorescence with a maximum at 503 nm upon excitation at 395 nm, due to a top-down etching process where the alkanethiol ligand was released after the substrate hydrolysis. Thus, based on the fluorescence enhancement, the concentration of esterase could be determined from 0.1 to 10 mU mL^{-1} with a detection limit of 0.04 mU mL^{-1}, and the concentration of ALP could be monitored between 0.01 and 10 mU mL^{-1}, with a detection limit of 0.005 mU mL^{-1} [123]. Also based on THPC-AuNPs, Chen et al. reported the synthesis of Cys-AuNCs by a ligand exchange method. The fluorescence of the obtained NCs (410 and 495 nm excitation and emission wavelengths, respectively) was quenched in the presence of Cu^{2+}, and further addition of pyrophosphate (PPi) gave rise to a fluorescence recovery due to the coordination of PPi with Cu^{2+}. Then, the addition of ALP to this mixture produced again a quenching of the luminescence, attributed to the hydrolysis of PPi by ALP. This methodology was applied to the detection of PPi and ALP, achieving detection limits of 2 mM and 0.1 mU/mL, respectively [124]. Another research group was used BSA-AuNCs as probe for the detection of proteases, which produced a quenching of the fluorescence due to the destruction of the protein shell that allowed the interaction of O_2 with the Au core. During the degradation of protein shell by protease enzyme, the O_2 can quickly interact with Au metal core, as a result of fluorescence quenching. A wide linear range for the detection of proteases was observed from 5 to 5×10^3 ng mL^{-1} [125].

There are several reports available in the literature for the detection of biological molecules. But, still the selectivity of biomolecule detection is challenging, because there are numerous coexisting biological compounds present in real samples. In this case, molecular-imprinted polymer-based probe is an interesting material to improve the selectivity. Further, the enzyme-coated NC also is a promising material to improve the selectivity. For example, uricase enzyme-coated NC probes achieved the good selectivity and sensitivity for the detection of uric acid [102, 103].

9.3.3 Detection of Drugs and Small Molecules

Detection of drugs is another important research topic where Au and AgNCs have been explored. Chloramphenicol is an antibiotic extensively used for the treatment of bacterial infections such as plague, cholera, meningitis, and typhoid fever. Hence, the detection of chloramphenicol is significant in clinical field. In this regard, 2 nm BSA-AuNCs were used to detect chloramphenicol, an antibiotic extensively used for the treatment of different diseases. Upon the addition of chloramphenicol, the fluorescence intensity of BSA-AuNCs was quenched at 650 nm due to the attachment of chloramphenicol on the surface of BSA-AuNCs by electrostatic interaction, giving rise to a photoinduced electron transfer. Based on this quenching, determination of this antibiotic can be performed in a linear range from 0.1 to 70 μM with a detection limit of 33 nM. Furthermore, this method was applied to detect chloramphenicol in milk samples. Most of the common interferents did not affect to the system [126]. Rifampicin is another antibiotic widely used for the

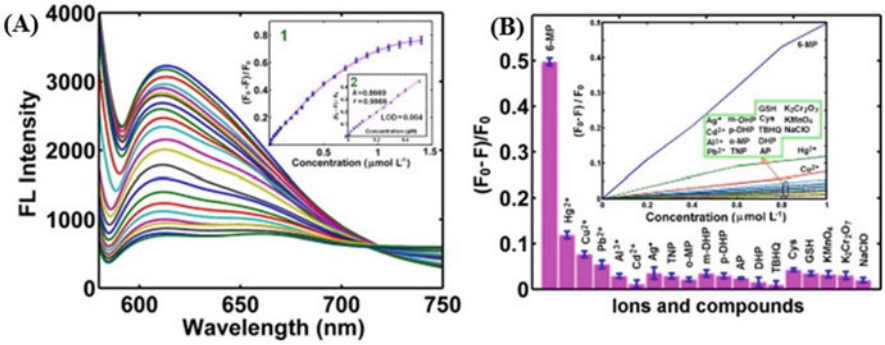

Fig. 9.9 (**a**) Fluorescence emission spectra of Fe_3O_4@SiO_2-AuNCs with different concentrations of 6-MP (from top to down, 0, 0.01, 0.02, 0.04, 0.06, 0.08, 0.10, 0.15, 0.20, 0.25, 0.30, 0.35, 0.40, 0.50, 0.60, 0.70, 0.80, 0.90, 1.00, 1.10, 1.20, 1.30, and 1.40 μM. *Insets*: *1*. calibration plot $(F_0 - F)/F_0$ versus concentration of 6-MP (0.01–1.40 μM) and *2*. plot of $(F_0 - F)/F_0$ versus low concentration of 6-MP (0–0.5 μM). (**b**) Selectivity study results of the proposed sensor for the analysis of 6-MP in B-R (pH = 8, 0.1 M; concentration of each interferent μM). *Inset*: Sensor responses to 6-MP and interferences at different concentrations (Reprinted by permission from Elsevier: [Biosensors and Bioelectronics] 70, 246–253. Copyright 2015)

treatment of cholestatic pruritus and tuberculosis. Once again, BSA-AuNCs (480 and 640 excitation and emission wavelengths, respectively) were used as probe for the detection of rifampicin based on a quenching of the luminescence, obtaining a linear response from 0.6 μM to 1 mM and a detection limit of 83.3 nM. In this work, a wax-printed paper platform was developed in order to perform real-time monitoring of rifampicin in urine samples [127].

In another application, Fe_3O_4@SiO_2 and BSA-AuNCs were prepared separately and coupled by COOH and NH_2 functional groups through the help of usual coupling agents such as 1-ethyl-3-(3-dimethylaminopropyl) carbodiimide (EDC) and N-hydroxysuccinimide (NHS) to generate Fe_3O_4@SiO_2@BSA-AuNCs. This probe shows a red emission at 613 nm with an excitation wavelength of 275 nm as depicted in Fig. 9.9. These NCs have shown high selectivity to the detection of 6-mercaptopurine versus other potential interferents including phenols, heavy metal ions, thiols, etc. During the addition of 6-mercaptopurine, it can be adsorbed on the surface of gold via thiol-Au bond. After the adsorption of 6-mercaptopurine, the AuNCs were destabilized due to the liberation of BSA from AuNCs. This increases the van der Waals attraction forces between the AuNCs and leads to aggregation of the particles, as a result of decrease in fluorescence. The methodology is based on the monitorization of the fluorescence intensity that is quenched after the addition of 6-mercaptopurine, with a linear response observed from 0.01 to 0.5 μM and a detection limit of 0.004 μM. The common interferents did not interfere for the detection of 6-mercaptopurine at pH 8 (Fig. 9.9b). This method was successfully applied for the detection of 6-mercaptopurine in lake water, human urine, and serum samples [128].

Fluorescence enhancement has been also exploited using BSA-AuNCs to detect naturally occurring amino acid of D-penicillamine. For this purpose, Cu^{2+} was added in order to aggregate the AuNCs and to quench the red emittive BSA-AuNCs at 650 nm when using an excitation wavelength of 514 nm. The addition of D-penicillamine generated a new complex of D-penicillamine-Cu^{2+}, and the aggregation state of the BSA-AuNCs disappeared giving rise to a restoration of their fluorescence. Based on this fluorescence enhancement, the detection of D-penicillamine in human serum samples was performed obtaining satisfactory results and a detection limit of 5.4 μM [129].

A similar approach was developed to monitor the presence of clioquinol, an antifungal drug. The clioquinol comes as a medical cream, lotion, and ointment, and it is commonly used to treat skin infections such as eczema, itch, and ringworm. Addition of Cu^{2+} quenched the fluorescence of BSA-AuNCs at 610 nm (λ_{ex}, 370 nm) and is due to the coordination of Cu^{2+} with the amino acid residues of BSA. Further, the obtained quenching revealed that the AuNCs excited state energy loss by intersystem crossing (ISC) process. The addition of Cu^{2+} containing BSA-AuNCs enhanced the fluorescence. It is expected that the obtained fluorescence enhancement is due to the binding of clioquinol with Cu^{2+}, and BSA-AuNCs were free from the binding of Cu^{2+}. Based on the fluorescence enhancement, the detection limit of clioquinol was found to be 0.63 μM, and good linearity was obtained from 1 to 12 μM of clioquinol [130]. Surface plasmon-enhanced energy transfer (SPEET) phenomenon between trypsin-AuNCs (try-AuNCs) and cysteine-AuNPs (cyst-AuNPs) is the principle employed for the detection of heparin. The try-AuNCs have shown an emission maximum at 690 nm upon excitation at 520 nm. After mixing cyst-AuNPs with try-AuNCs, the fluorescence of the NCs was quenched, and upon the addition of heparin, the luminescent emission was restored. The positively charged cyst-AuNPs could bind with negatively charged heparin. Due to their electrostatic interaction, SPEET can be collapsed. As a result, the enhancement of try-AuNC fluorescence was observed, because of try-AuNC liberation from the binding. The detection of heparin provided a linear response from 0.1 to 4 μg/mL and a detection limit of 0.05 μg/mL. Moreover, further modification of try-AuNCs with folic acid was used for in vivo cancer imaging [86].

BSA-AuNCs were used for the detection of one of the protein cross-linkers glutaraldehyde in tap and river water samples using excitation and emission wavelengths at 370 nm and 621 nm, respectively. The methodology was based on monitorization the quenching of the luminescence due to an aggregation of BSA-AuNCs in the presence of glutaraldehyde, and it has allowed to perform the detection between 0.8 and 6 μM, with a detection limit of 0.2 μM [131]. Methotrexate detection was also performed based on the quenching of the luminescence of BSA-AuNCs at 633 nm upon excitation at 480 nm. This method has allowed the detection of methotrexate in the range of 3.5 μM–55 mM in real samples including human urine and serum, with a detection limit for methotrexate of 2 nM [132].

Another area where the use of metallic nanoclusters is the detection of small molecules including nitric oxide, salicylaldehyde, urea and sodium dodecyl sulfate,

poly diallyldimethyl ammonium chloride, etc. In this case, most of the applications reported in the literature are based on the use of well-known nanoclusters, namely, BSA-capped AuNCs. Recently, a detection of nitric oxide (NO) was performed with BSA-AuNCs as probe based on a quenching effect monitored at 640 nm when the excitation is at 470 nm. It was deduced that the quenching of BSA-AuNC fluorescence may be the interaction between NO and BSA. A liner range is observed between 50 μM and 350 μM addition of NO and achieved a detection limit of 17 μM [133].

BSA-AuNCs also were used as probe for the detection of salicylaldehyde (SA) and Zn^{2+}. After the addition of SA, the fluorescence intensity of BSA-AuNCs was quenched at 640 nm, and this effect was ascribed to the formation of a Schiff base (C = N bond) between an amino functional group from BSA and an aldehyde group from SA. Moreover, a new well-resolved fluorescence maximum appeared at lower wavelength (500 nm), and a change on the color of the liquid dispersion from red to green was also observed under UV light (Fig. 9.10). Zn^{2+} is further introduced into the system and the color of the solution was changed from red to lavender, and this is attributed to the formation of SA-Zn^{2+} complex due to the strong coordination of Zn^{2+} with C = N and OH groups of SA. Further, addition of Zn^{2+} leads to quench the fluorescence at 640 nm and is enhanced at 500 nm with blueshift (Fig. 9.10). Thus, based on this double effect of fluorescence quenching and enhancement, the concentration of SA was determined successfully from 15.8 μM to 1.58 mM (LOD of 0.19 μM) at 500 nm and from 0.1 μM to100 μM in the case of Zn^{2+} detection (LOD of 29.28 nM) [134].

Further, detection of urea was developed by Lakshmi et al. using mercaptosuccinic acid (MSA)-capped gold nanoparticles that after reaction with GSH at pH 1.5 under 70 °C for 24 h gave rise to double-ligand fluorescent MSA-GSH-AuNCs. Furthermore, MSA-GSH-AuNCs were coated with urease enzyme and applied to the detection of urine in blood samples from 2.5 to 10 mM that produced a quenching of the fluorescence due to aggregation of the nanoclusters confirmed by TEM. The major interferents such as cysteine and homocysteine did not interfere in this system. Moreover, this method was applied to detect the urea in blood serum sample [135].

Finally, 1.2-nm-sized GSH-AuNCs (410 and 660 nm excitation and emission wavelengths, respectively) were used as probe for the detection of poly diallyldimethyl ammonium chloride (PDDA) that generated a fluorescence enhancement due to electrostatic repulsion. Interestingly, the addition of sodium dodecyl sulfate (SDS) gave rise to a quenching of the fluorescence attributed to the strong affinity of PDDA and SDS (Fig. 9.11). PDDA could be monitored at concentrations between 0.2 and 12 mg mL^{-1} with a detection limit of 0.02 mg mL^{-1} [136].

In this section, we have discussed the small molecule and drug detection using silver and gold nanoclusters. There are numerous reports available for the detection of small molecules and drugs, but still there is an urgent need to develop some essential drug sensors, for example, HIV drugs of nevirapine, rilpivirine, and etravirine and other important drugs of morphine, aspirin, penicillin, etc. More

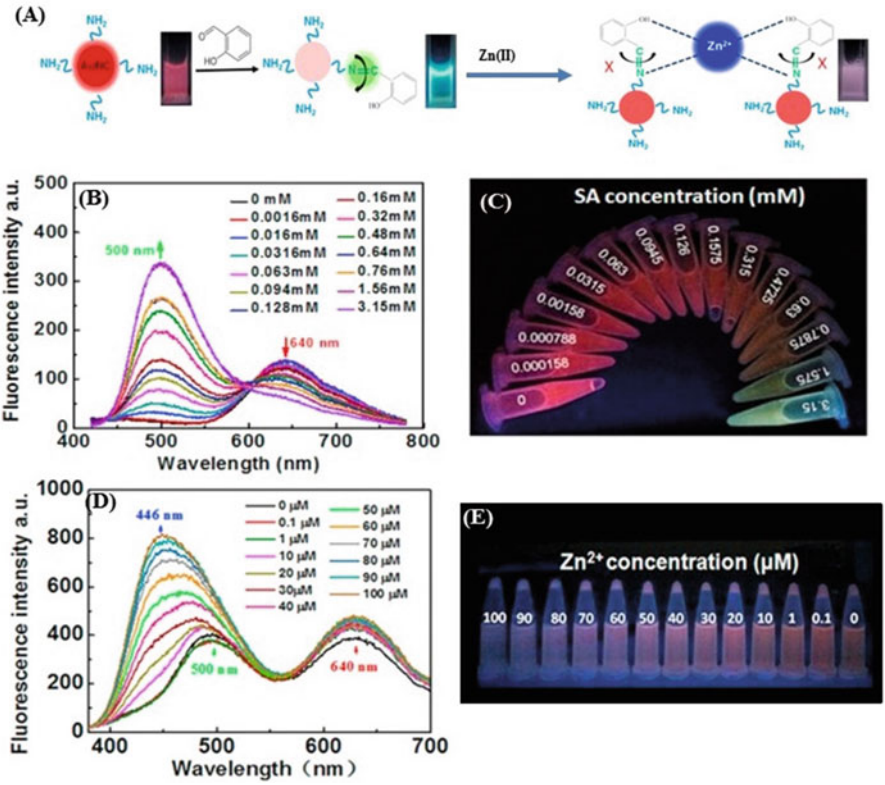

Fig. 9.10 (**a**) Schematic illustration of the fluorescence switching strategy for detection of SA and Zn^{2+}. (**b**) The emission spectra of BSA-AuNCs in the presence of different concentrations of SA and (**c**) corresponding photographic image of the samples under UV lamp irradiation ($\lambda_{ex} = 365$ nm). (**d**) The fluorescence emission spectra of BSA-AuNCs in the presence of 0.64 mM SA with different concentrations of Zn^{2+}. (**e**) Corresponding photographic images of the samples under UV lamp irradiation ($\lambda_{ex} = 365$ nm) (Reprinted by permission from Elsevier: [Biosensors and Bioelectronics] 74, 322–328. Copyright 2015)

researches are needed to do in this drug sensor field, and it is important to develop portable kit for the small molecules and drug sensor for real sample analysis.

9.3.4 Detection of Toxic Chemicals

The detection of toxic chemicals is important to protect the living beings from their hazards. Continuous exposure of toxic chemicals can be a threat to the human beings. Hence, detection is very important today. For example, tea polyphenol sensing was performed by Sainan et al. due to the aggregation of BSA-AuNCs. The tea polyphenols interact with Au metal core and lead to aggregate the AuNCs,

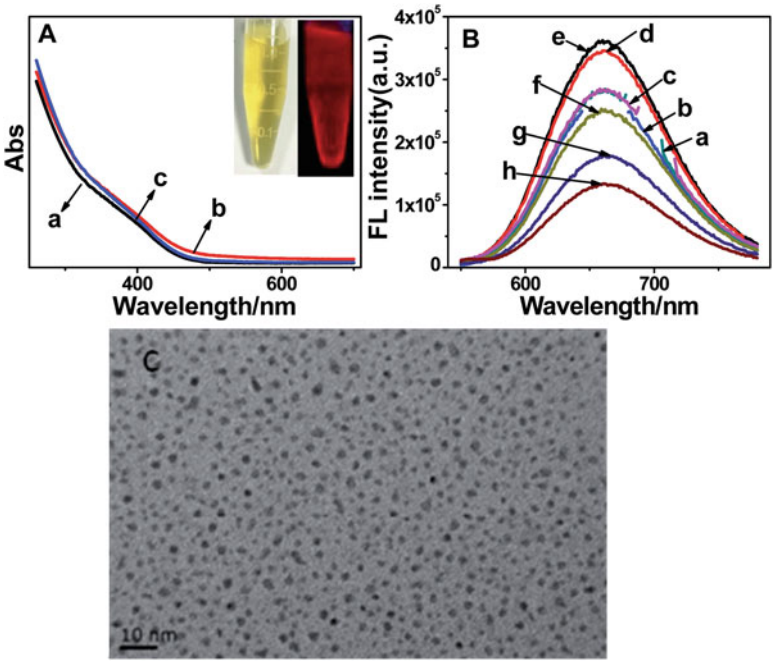

Fig. 9.11 (**a**) UV-vis absorption spectrum of the GSH-AuNCs (**a**) and GSH-AuNCs/PDDA (**b**) GSH-AuNCs/PDDA/SDS (**c**). Concentrations: GSH-AuNCs (50 μg mL^{-1}), PDDA (12.5 μg mL^{-1}), and SDS (2 μg mL^{-1}). *Inset*: photographs of an aqueous solution of GSH-AuNCs in visible light (*left*) and UV light (*right*). (**b**) Fluorescence spectra of the GSH-AuNCs at different excitation wavelengths (a–h, 330, 340, 350, 390, 410, 420, 450, 470 nm). Concentration: GSH-AuNCs (0.2 mg mL − 1) (**c**) typical TEM image of GSH-AuNCs (Reprinted by permission from The Royal Society of Chemistry: [Analyst], 139, 3476–3480. Copyright 2014)

the quenching of the luminescence that allowed the detection of these polyphenols in tea samples with a detection limit of 10 nM. Good linearity was observed from 10 μM to 10 nM addition of tea polyphenols. Finally, this system was applied for the detection of tea polyphenol in tea samples [137]. The same type of BSA-AuNCs was used as probe for the detection of hypochlorite. In this work, the fluorescence of BSA-AuNCs was quenched upon addition of HOCl at 640 nm (λ_{ex}, 480 nm) due to a selective oxidation of the amino acid residues of BSA. A detection limit of 100 nM was achieved, and the methodology was successfully applied to the detection of HOCl in tap water samples [138].

Melamine is a nitrogen rich toxic chemical and shows the analytical characteristics of protein by Kjeldahl method. Hence, the unethical manufactures used it for adulterate protein-rich diets in milk, milk powder, biscuits, etc. The melamine-contaminated foods can produce insoluble stones in the kidney for animals and humans. Thus, their detection is significant today. In this regard, Dai et al. have developed the method for the detection of melamine using BSA-AuNC probe.

It shows the emission maximum at 640 nm upon excitation at 410 nm. The fluorescence of BSA-AuNCs was quenched during the addition of Hg^{2+}, and further addition of melamine produced a recovery of the fluorescence due to the coordination of Hg^{2+} with melamine. Good linearity was observed from 0.5 to 10 μM, and a detection limit of 0.15 μM was achieved. This system was successfully applied for the detection of melamine in milk and milk powder samples [139]. Xin et al. has been reported that the rapid detection of nitro aromatic explosives of 2,4,6-trinitrotoluene (TNT) and 4-nitrophenol (4-NP) using BSA-AuNCs. The detection is again based on the quenching of the luminescence due to the interaction between the electron-withdrawing nature of the nitro group present in TNT and 4-NP with BSA-AuNCs. Good linearity for TNT and 4-NP was obtained from 10 nM to 50 μM and 1 nM to 50 μM and detection limits of 10 nM and 1 nM, respectively. Moreover, high selectivity was achieved for the detection of TNT and 4-NP even in the presence of other potential interferents including nitro aromatic compounds. Further, the test paper-coated probe was developed to demonstrate the detection of TNT and 4-NP [140].

Molecular-imprinted polymer AuNCs (MIP@GSH-AuNCs) were fabricated by four-step process and used for the detection of bisphenol A. Firstly, GSH-capped AuNCs were synthesized with carboxyl functional group by GSH as stabilizing agent. On the other hand, amine functionalized SiO_2 coating was generated using tetraethyl orthosilicate (TEOS) and (3-aminopropyl)triethoxysilane (APTES), and then it was coupled with carboxyl functionalized GSH-AuNCs by using EDC and NHS coupling chemistry, and the result obtained a highly fluorescent SiO_2@GSH-AuNC. The MIP solution was prepared by stirring APTES and bisphenol for 12 h, and then SiO_2@AuNCs dispersed in PBS at pH 7 were mixed with the previous solution and stirred for 30 min. NH_3, H_2O, and TEOS were added and stirred for 12 h, and then the bisphenol A was removed from template of MIP (Fig. 9.12). The synthesized MIP@GSH-AuNCs were used as probe for the detection of bisphenol A, which produced a highly selective quenching of the luminescence once the bisphenol A interacted with the MIP@GSH-AuNCs. The detection limit obtained was found to be 100 nM, and the methodology was successfully evaluated in sea water samples [141].

9.3.5 Detection of Bacteria

Bacteria can cause food poisoning. The symptoms of food poisoning will be varied, which depends on the nature of bacteria. Salmonella, norovirus, campylobacter, *E. coli*, and listeria are the major types of bacteria. *Staphylococcus aureus* bacteria was detected by vancomycin antibody-coated AuNCs (V-AuNCs). Firstly, V-AuNCs were prepared by one-step process. In briefly, $HAuCl_4$ was stirred with water in a beaker and it was heated at 100 °C. Then vancomycin was added into the mixture and continued to heat at 100 °C for 50 min. Then the obtained V-AuNCs were purified by the centrifugation. The resultant V-AuNCs exhibit the emission

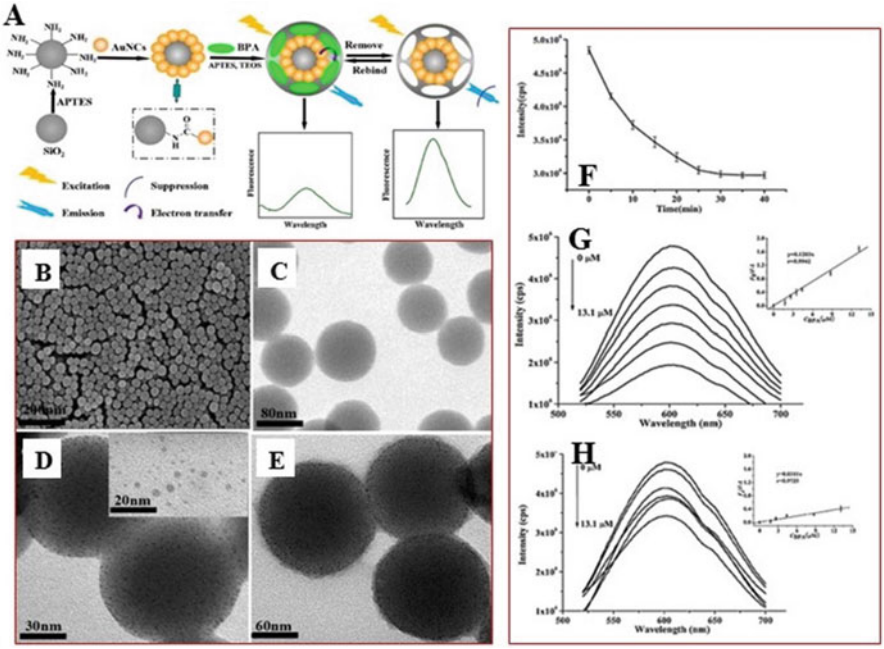

Fig. 9.12 (**a**) Schematic illustration of the process for the preparation of the SiO_2@AuNCs-MIPs. (**b**) SEM image and (**c**) TEM image of SiO2, (**d**) TEM image of SiO_2@AuNCs (*inset d*: TEM image of AuNCs) (**e**) TEM image of SiO_2@AuNCs-MIPs. (**f**) Fluorescence response time of SiO_2@AuNCs-MIPs for BPA. (**g**, **h**): Fluorescence emission spectra of SiO_2@AuNCs-MIPs and SiO_2@AuNCs-NIPs with addition of the indicated concentrations of BPA, respectively. The inset graphs show fluorescence intensity corresponding Stern-Volmer plots. The experimental conditions were SiO_2@AuNCs-MIP or SiO_2@AuNCs-NIP 25 mg/L; CBPA, 3.4 μM; and excited light, 396 nm (Reprinted by permission from Elsevier: [Sensors and Actuators B-Chemical] 211, 507–514. Copyright 2015)

maximum at 410 nm when using an excitation wavelength of 303 nm. The QY obtained for these nanoclusters was 3%, and the luminescence was quenched upon addition of *Staphylococcus aureus* due to its binding to V-AuNCs. Based on the quenching of fluorescence, detection of *Staphylococcus aureus* was performed in milk and serum samples with a high sensitivity (detection limit of 16 cfu/mL) [142].

Red emittive lysozyme and L-cysteine dual ligand-capped fluorescent AuNCs (Ly@Cy-AuNCs) were synthesized by Jiali et al. This nanocluster was exhibiting emission at 610 nm with an excitation wavelength at 365 nm. This Ly@Cy-AuNC was used as probe for the detection of *Escherichia coli* (*E. coli*). The obtained fluorescence enhancement revealed the interaction of *E. coli* with lysozyme of Ly@Cy-AuNCs (Fig. 9.13), and it provides a linear range between 2.4×10^4 and 6.0×10^6 cfu/mL and a detection limit of 2.0×10^4 cfu/mL [143].

Further, human serum albumin-stabilized AuNCs (HAS-AuNCs) showing red emission under UV light (367 and 640 nm excitation and emission wavelengths,

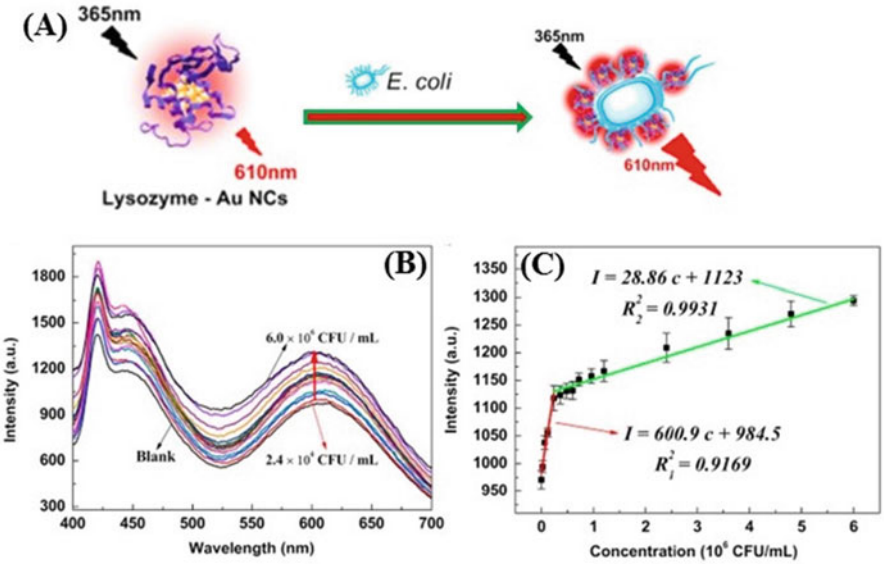

Fig. 9.13 (**a**) Schematic representation of the red fluorescent lysozyme-AuNCs and fluorescence enhancement detection of *E. coli*. (**b**) Evolution of red fluorescence spectra of lysozyme-AuNCs vs *E. coli* concentrations. (**c**) The calibration plots of red fluorescence intensity vs *E. coli* concentrations, $\lambda_{ex}/\lambda_{em}$ = 365/610 nm. Lysozyme-AuNCs, 50.0 μM; buffer solution, Tris-HCl (pH 6.0, 20.0 mM) (Reprinted by permission from Elsevier: [Talanta] 134, 54–59. Copyright 2015)

respectively) were evaluated as probe for the detection of pathogenic bacteria including *Staphylococcus aureus* and methicillin-resistant *Staphylococcus aureus* (MRSA). The fluorescence of HAS-AuNCs was quenched in the presence of these bacteria due to a binding between the peptides of HSA and the bacteria. The detection limit by naked eye was found to be $\sim 10^6$ cells/mL [144]. H-Tchang et al. reported the synthesis of 11-mercapto-3,6,9-trioxaundecyl-r-D-mannopyranoside-protected AuNDs (Man-AuNDs) from THPC-AuNP precursors via a ligand exchange method. Further it was used for the detection of *E. coli* and concanavalin A (Con A, a carbohydrate-binding protein). Man-AuNDs showing emission maximum at 545 nm upon excitation at 365 nm generated an enhancement of the luminescence after addition of Con A. Moreover, Man-AuND was evaluated as probe for the detection of *E. coli* bacteria, since it stabilizes the formation of stable fluorescent aggregated clusters due to multivalent interactions between the mannosylated AuNDs and mannose receptors located on the bacterial pili. This aggregation led to a fluorescence enhancement of Man-AuNDs, which was exploited to detect *E. coli* between 1.00×10^6 and 5.00×10^7 cells/mL, with the detection limit of *E. coli* of 7.20×10^5 cells/mL [145]. Generally the bacteria detection can be done by using of antibody, aptamer, antibiotic, etc. Among them, antibody- and aptamer-coated probes are effective, because they have high specificity and sensitivity and are easy to synthesize. In Table 9.3,

Table 9.3 Summary of methodologies reported for the detection of biomolecules, small molecules, enzymes, and toxic chemicals and bacteria using Au/AgNCs with sensing mechanism

Analyte	NCs or NDs	$\lambda_{ex/em}$	Linear range	LOD	Sensing mechanism	Real sample	References
Ascorbic acid	BSA-AuNCs	270/620 nm	1.5–10 nM	0.2 mM	Interaction with metal core	Plasma samples	[84]
Heparin	Trypsin-AuNCs	520/690 nm	0.1–4 μg/mL	0.05 μg/mL	Indirect approach	Human serum	[86]
Folic acid	BSA-AuNCs	505/652 nm	0.11–2.27 μM	0.065 μM	Ligand-induced aggregation	Tablets and human blood serum	[87]
Folic acid	BSA-AuNCs	365/640 nm	0.27–4.5 μM	45 nM	Ligand-induced charge transfer	Bioimaging studies in tumor cells	[88]
Cysteamine	BSA-AuNCs	650 nm	0.5–10 μM	150 nM	Interaction with metal core	Human serum samples	[89]
L-Cysteine	PDMAM-AuNPs@ BSA-AuNCs	503/620 nm	5–50 mM	3.6 μM	Ligand-induced charge transfer	Urine	[90]
Cysteine and Glutathione	BSA-Ag@AuNCs	370/650 nm	20–80 nM and 2–70 nM for cysteine and glutathione respectively	5.87 nM and 1.01 nM for cysteine and GSH, respectively	Interaction with metal core	Human plasma samples	[91]
Glutathione	Mt@MUA-AuNCs	275/608 nm	30 nM–22.5 μM	9.7 nM	Indirect approach	Hep G2 cells (human liver cancer cells)	[92]
Glutathione	BSA-AuNCs	530/670 nm	0.04–16.0 μM	7.0 nM	Ligand decomposition	Living cells and human blood samples	[93]

(continued)

Table 9.3 (continued)

Analyte	NCs or NDs	$\lambda_{ex/em}$	Linear range	LOD	Sensing mechanism	Real sample	References
Trypsin	BSA-AuNCs	385/650 nm	0.01–100 μg/mL	2 ng/mL	Ligand decomposition	Human urine	[94]
Mitoxantrone	GSH-AuNCs	392/570 nm	0.1–6 μm	20 nM	Ligand-induced charge transfer	Human urine	[96]
ATP and pyrophosphate	GSH-AuNCs	396/613 nm	50–500 μM for ATP and from 50 to 100 μM for pyrophosphate	~43 μM and ~28 μM for ATP and pyrophosphate, respectively	Ligand-induced charge transfer	Human blood plasma	[98]
NADH	Trypsin-AgNCs	580/662 nm	10–300 μM	5 μM	Ligand-induced charge transfer	Bovine serum	[99]
Hemoglobin	MUA-AuNDs	375/520 nm	1–10 nM	0.5 nM	Interaction with metal core	Human serum	[100]
Cholesterol	BSA-AuNCs	350/635 nm	N/R	12 μM	Interaction with metal core	N/R	[101]
Uric acid	BSA-AuNCs@uricase enzyme	370/610 nm	10–800 μM	6.6 μM	Ligand-induced charge transfer	Human serum	[102]
Uric acid	BSA-AuNCs@ urate oxidase enzyme	365/600	0.7–80 μM	120 nM	Interaction with metal core	Human serum	[103]
Dopamine	BSA-AuNCs	500/615 nm	10 nM–1 μM	10 nM	Ligand-induced charge transfer	Human serum	[104]
Dopamine and tyrosinase	GSH-AuNCs	350/610 nm	N/R	0.006 unit mL^{-1} for tyrosinase and 1.0 nM for dopamine	Ligand-induced aggregation	Dopamine injection	[105]
Acid phosphatase	GSH/MUA-AuNCs	293/610 nm	N/R	1 nM	Indirect approach	N/R	[106]
Glucose	BSA-AuNCs@ glucose oxidase	390/650 nm	10 μM–0.5 mM	5 μM	Interaction with metal core	Blood serum	[110]
Glucose	Ovalbumin-AuNCs	625 nm	5 μM–10 mM	1 μM	Ligand decomposition	Urine	[111]

Protein kinase II	Peptide-AuNCs	325/414 nm	0.08–2 unit mL^{-1}	0.027 unit mL^{-1}	Ligand-induced aggregation	Blood serum	[119]
Glutathione S-transferase	GSH-AuNCs	590/824 nm	2–100 nM	1.5 nM	Ligand-induced charge transfer	N/R	[120]
Acetylcholines-terase	Denatured BSA	520/640 nm	0.005 and 0.15 UmL^{-1}	0.02 $mUmL^{-1}$	Interaction with metal core	Blood serum	[121]
Phospholipase C	MUA-AuND/Lip hybrids	370/530 nm		0.21 nM	Indirect approach	N/R	[122]
Esterase and alkaline phosphatase (ALP)	MH-AuNCs	395/503 nm	0.1–10 mU mL^{-1} for esterase and 0.01 and 10 mU mL^{-1} for ALP	0.04 mU mL^{-1} for esterase and 0.005 mU mL^{-1} for ALP	Indirect approach	Calf serum	[123]
Pyrophosphate (PPi) and ALP	Cys-AuNCs	410/495 nm	N/R	2 mM and 0.1 mU/mL for pyrophosphate (PPi) and ALP, respectively	Interaction with metal core	N/R	[124]
Proteases	BSA-AuNCs	500/650 nm	5–5 × 10^3 ng mL^{-1}	1 ng/mL	Ligand decomposition	N/R	[125]
Chloramphenicol	BSA-AuNCs	260/650 nm	0.1–70 μM	33 nM	Ligand-induced charge transfer	Milk	[126]
Rifampicin	BSA-AuNCs	480/640 nm	0.6 μM–1 mM	83.3 nM	Ligand-induced charge transfer	Urine	[127]
Mercaptopurine	Fe_3O_4@SiO_2 @BSA-AuNCs	275/613 nm	0.01–0.5 μM	0.004 μM	Interaction with metal core	Lake water, human urine, and serum samples	[128]
Penicillamine	BSA-AuNCs	514/650 nm	20–230 μM	5.4 μM	Indirect approach	Human serum	[129]
Clioquinol	BSA-AuNCs	370/610 nm	1–12 μM	0.63 μM	Indirect approach	Clioquinol cream samples	[130]
Glutaraldehyde	BSA-AuNCs	370/621 nm	0.8 and 6 μM	0.2 μM	Ligand decomposition	Tap and river water	[131]

(continued)

Table 9.3 (continued)

Analyte	NCs or NDs	$\lambda_{ex/em}$	Linear range	LOD	Sensing mechanism	Real sample	References
Methotrexate	BSA-AuNCs	480/633 nm	3.5 μM–55 mM	2 nM	Ligand-induced charge transfer	Human urine and serum	[132]
Nitric oxide (NO)	BSA-AuNCs	470/640 nm	50–350 μM	17 μM	Ligand decomposition	N/R	[133]
Salicylaldehyde (SA) and Zn^{2+}	BSA-AuNCs	640 nm and 500 nm	15.8 μM–1.58 mM for SA and 0.1 μM–100 μM for Zn^{2+}	0.19 μM and 29.28 nM for SA and Zn^{2+}, respectively	Ligand-induced aggregation	Blood serum	[134]
Sodium dodecyl sulfate	GSH-AuNCs	410/660 nm	0.2 and 12 mg mL^{-1}	0.02 mg mL^{-1}	Ligand-induced charge transfer	N/R	[136]
Tea polyphenol	BSA-AuNCs	375/625 nm	10 μM–10 nM	10 nM	Interaction with metal core	Tea	[137]
Hypochlorous acid (HOCl)	BSA-AuNCs	480/640 nm	0.34–17.2 μM	100 nM	Ligand-induced charge transfer	Tap water	[138]
Melamine	BSA-AuNCs	410/640 nm	0.5–10 μM	0.15 μM	Ligand decomposition	Milk and milk powder	[139]
Trinitrotoluene and nitrophenol	BSA-AuNCs	260/358 nm	10 nM–50 μM and 1 nM–50 μM for TNT and 4-NP, respectively	10 nM and 1 nM for TNT and 4-NP, respectively	Ligand-induced charge transfer		[140]
Bisphenol A	MIP@GSH-AuNCs	396/600 nm	N/R	100 nM	Ligand-induced charge transfer	Sea water	[141]
Staphylococcus bacteria	V-AuNCs	303/410 nm	N/R	16 cfu/mL	Ligand-induced aggregation	Milk and serum samples	[142]
E. coli bacteria	Ly@Cy-AuNCs	365/610 nm	2.4×10^4 and 6.0×10^6 cfu/mL	2.0×10^4 cfu/mL	Ligand-induced aggregation	N/R	[143]
Staphylococcus aureus and *Staphylococcus aureus* bacteria	HAS-AuNCs	367/640 nm	N/R	1×10^6 cells/mL	Ligand-induced aggregation	N/R	[144]
E. coli bacteria and concanavalin A	Man-AuNDs	365/545 nm	1.00×10^6 and 5.00×10^7 cells/mL	7.20×10^5 cells/mL	Ligand-induced aggregation	N/R	[145]

N/R not reported

we have summarized the application of Au/AgNCs for the detection of biomolecules, small molecules, enzymes, toxic chemicals and bacteria, linear range, detection limit, sensing mechanism, and type of real sample evaluated.

9.4 Conclusions and Trends

Metal NCs with size below 1.5 nm and NDs with size between 1.5 and 3 nm are a novel class of fluorescent nanomaterials [146]. Because of their fascinating physical and chemical properties such as ultrasmall size, higher surface area, biocompatibility, catalytic efficiency, higher luminescence, low photobleaching, and higher solubility in aqueous media which allowed them to be used as attractive fluorescent materials in various applications including toxic and biochemical sensing, bioimaging, phototherapy, and catalysis etc., Recent advances in synthesis of fluorescent nanomaterials by different methods including top-down and bottom-up strategies have contributed to understand the fundamental physical and chemical properties of fluorescent nanomaterials. However, these fluorescent nanomaterials are being increasingly explored as sensing probes for many different types of analytes; further advancement and research on these fluorescent nanomaterials need to be performed, facing a variety of tasks. There is still a need to develop facile room temperature and one-pot synthesis routes of fluorescent nanomaterials with high quantum yield. However, most of the reported fluorescent nanomaterials are synthesized at very high temperatures or controlled at 37 °C with long reaction times that take up to several days. Moreover, in general terms, the fluorescent QYs reported are rather low (typically below 10%) [35], in comparison with many organic dyes and other types of fluorescent nanomaterials such as semiconductor quantum dots. Hence, it is essential to develop a very simple synthesis route to obtain fluorescent nanomaterials with a short period of time at room temperature and high QY. Further, the developed method can be performed in the laboratory without the need of sophisticated equipment. In this regard, Vasimalai et al. recently reported the new protocol for the synthesis of one-pot and room temperature-mediated AuNDs within 10 min, with a QY of ∼10% [77], that already overcome the main drawbacks of the majority of the synthesis reported in the literature. These results may spawn new strategies for future progress in this direction.

Secondly, many of the applications reported so far are based on a quenching or enhancement effect due to electrostatic interactions of the nanomaterials with the analytes or to aggregation/disaggregation of the nanoclusters that might take place with several compounds of similar nature. Therefore, there are still selectivity issues that should be improved in order to extend the application of this type of fluorescent nanomaterials as sensing probes. In this sense, the use of a selective or specific recognition element conjugated to the nanoclusters, such as antibodies or antigens to perform fluorescent immunoassays, or the use of aptamers or MIPs is a topic that will generate highly selective applications in the near future. Besides the use of these nanomaterials as sensing probes, there is a trend to impart more functionalities to the nanomaterial. So far, the designing of fluorescent nanomaterials with good

biocompatibility and good aqueous solubility is thus being a perfect candidate for biomedical applications. In this sense, the synthesis of nanomaterials that also includes other features, such as magnetic or thermal properties, will allow the use of these nanomaterials as sensing probes and magnetic resonance imaging (MRI) or photothermal agents for therapeutic applications.

In summary, the synthesis and biochemical and sensing applications of these fluorescent nanomaterials are still at an early stage, and much work needs to be done. The attractive features of these ultrasmall fluorescent nanomaterials including NCs and NDs. Together with the new advances in the synthesis and surface modifications, will spread their use in the next years in a wide variety of fields, including sensing applications, drug delivery, therapy and molecular diagnosis, etc.

References

1. K. Saha, S.S. Agasti, C. Kim, X. Li, V.M. Rotello, Gold nanoparticles in chemical and biological sensing. Chem. Rev. **112**(5), 2739–2779 (2012)
2. D. Diamond, *Principles of Chemical and Biological Sensors* (Wiley, New York, 1998)
3. O.A. Sadik, W.H. Land, J. Wang, Targeting chemical and biological warfare agents at the molecular level. J. Electroanal. **15**, 1149–1159 (2003)
4. M.R. Hormozi-Nezhad, E. Seyedhosseini, H. Robatjazi, C. Iranica, Spectrophotometric determination of glutathione and cysteine based on aggregation of colloidal gold nanoparticles. Sci. Iran. **19**, 958–963 (2012)
5. X. Chen, C. Han, H. Cheng, Y. Wang, J. Liu, Z. Xu, L. Hu, Rapid speciation analysis of mercury in seawater and marine fish by cation exchange chromatography hyphenated with inductively coupled plasma mass spectrometry. J. Chromatogr. A **1314**, 86–93 (2013)
6. H. Cheng, C. Wu, J. Liu, Z. Xu, Thiol-functionalized silica microspheres for online preconcentration and determination of mercury species in seawater by high performance liquid chromatography and inductively coupled plasma mass spectrometry. RSC Adv. **5**, 19082–19090 (2015)
7. A.L. Sanford, S.W. Morton, K.L. Whitehouse, H.M. Oara, L.Z. Lugo-Morales, J.G. Roberts, L.A. Sombers, Voltammetric detection of hydrogen peroxide at carbon fiber microelectrodes. Anal. Chem. **82**(12), 5205–5210 (2010)
8. Y. Ji, N. Leymarie, D.J. Haeussler, M.M. Bachschmid, C.E. Costello, C. Lin, Direct detection of S-palmitoylation by mass spectrometry. Anal. Chem. **85**, 11952–11959 (2013)
9. V.A. Lemos, S. Novaes Gdos, A.L. de Carvalho, E.M. Gama, A.G. Santos, Determination of copper in biological samples by flame atomic absorption spectrometry after precipitation with Me-BTAP. Environ. Monit. Assess. **148**, 245–253 (2009)
10. N. Ding, Q. Cao, H. Zhao, Y. Yang, L. Zeng, Y. He, K. Xiang, G. Wang, Colorimetric assay for determination of lead(II) based on its incorporation into gold nanoparticles during their synthesis. Sensors **10**, 11144–11155 (2010)
11. J. Li, Y. Li, D. Xu, J. Zhang, Y. Wang, C. Luo, Determination of metrafenone in vegetables by matrix solid-phase dispersion and HPLC-UV method. Food Chem. **214**, 77–81 (2017)
12. X. Qu, Y. Li, L. Li, Y. Wang, J. Liang, J. Liang, Fluorescent gold nanoclusters: Synthesis and recent biological application. J. Nanomater. **2015**, 784097 (2015)
13. J. Chena, X. Zhang, S. Cai, D. Wu, M. Chen, S. Wang, J. Zhang, A fluorescent aptasensor based on DNA-scaffolded silver-nanocluster for ochratoxin A detection. Biosens. Bioelectron. **57**, 226–231 (2014)

14. C.A.J. Lin, C.H. Lee, J.T. Hsieh, H.H. Wang, J.K. Li, J.L. Shen, W.H. Chan, H.I. Yeh, W.H. Chang, Synthesis of fluorescent metallic nanoclusters toward biomedical application: Recent progress and present challenges. J. Med. Biol. Eng. **29**(6), 276–283 (2009)
15. P. Yu, X. Wen, Y.-R. Toh, X. Ma, J. Tang, Fluorescent metallic nanoclusters: Electron dynamics, structure, and application. Part. Part. Syst. Charact. **32**, 142–163 (2015)
16. R. Jin, Quantum sized, thiolate-protected gold nanoclusters. Nanoscale **2**, 343–362 (2010)
17. Z. Wu, R. Jin, On the ligand's role in the fluorescence of gold nanoclusters. Nano Lett. **10**, 2568–2573 (2010)
18. C.M. Aikens, Electronic structure of ligand-passivated gold and silver nanoclusters. J. Phys. Chem. Lett. **2**, 99–104 (2011)
19. P.D. Jadzinsky, G. Calero, C.J. Ackerson, D.A. Bushnell, R.D. Kornberg, Structure of a thiol monolayer-protected gold nanoparticle at 1.1 A resolution. Science **318**, 430–433 (2007)
20. M.W. Heaven, A. Dass, P.S. White, K.M. Holt, R.W.J. Murray, Crystal structure of the gold nanoparticle $[N(C_8H_{17})_4][Au_{25}(SCH_2CH_2Ph)_{18}]$. J. Am. Chem. Soc. **130**, 3754–3755 (2008)
21. C. Zeng, H. Qian, T. Li, G. Li, N.L. Rosi, B. Yoon, R.N. Barnett, R.L. Whetten, U. Landman, R. Jin, Total structure and electronic properties of the gold nanocrystal $Au_{36}(SR)_{24}$. Angew. Chem. Int. Ed. **51**, 13114–13118 (2012)
22. Z. Luo, K. Zheng, J. Xie, Engineering ultrasmall water-soluble gold and silver nanoclusters for biomedical applications. Chem. Commun. **50**, 5143–5155 (2014)
23. R.W. Murray, Nanoelectrochemistry: Metal nanoparticles, nanoelectrodes, and nanopores. Chem. Rev. **108**, 2688–2720 (2008)
24. C. Zeng, T. Li, A. Das, N.L. Rosi, R. Jin, Chiral structure of thiolate-protected 28-gold-atom nanocluster determined by X-ray crystallography. J. Am. Chem. Soc. **135**, 10011–10013 (2013)
25. M. Zhu, H. Qian, X. Meng, S. Jin, Z. Wu, R. Jin, Chiral Au_{25} nanospheres and nanorods: Synthesis and insight into the origin of chirality. Nano Lett. **11**, 3963–3969 (2011)
26. P.-C. Chen, P. Roy, L.-Y. Chen, R. Ravindranth, H.-T. Chang, Gold and silver nanomaterials-based optical sensing systems. Part. Part. Syst. Charact. **31**, 917–942 (2014)
27. J. Zheng, C. Zhou, M. Yu, J. Liu, Different sized luminescent gold nanoparticles. Nanoscale **4**, 4073–4083 (2012)
28. A. Mooradian, Photoluminescence of metals. Phys. Rev. Lett. **22**, 185–187 (1969)
29. D. Lee, R.L. Donkers, G. Wang, A.S. Harper, R.W. Murray, Electrochemistry and optical absorbance and luminescence of molecule-like Au_{38} nanoparticles. J. Am. Chem. Soc. **126**, 6193–6199 (2004)
30. J.P. Wilcoxon, B.L. Abrams, Synthesis, structure and properties of metal nanoclusters. Chem. Soc. Rev. **35**, 1162–1194 (2006)
31. Z. Yuan, Y. Du, Y.T. Tseng, M. Peng, N. Cai, Y. He, H.T. Chang, E.S. Yeung, Fluorescent gold nanodots based sensor array for proteins discrimination. Anal. Chem. **87**, 4253–4259 (2015)
32. M. Cui, Y. Zhao, Q. Song, Synthesis, optical properties and applications of ultra-small luminescent gold nanoclusters. Trends Anal. Chem. **57**, 73–82 (2014)
33. S. Zhu, Y. Zhuo, H. Miao, D. Zhong, X. Yang, Detection of mercury(II) by DNA templated gold nanoclusters based on forming thymidine-Hg(2+)-thymidine duplexes. Luminescence **30**, 631–636 (2015)
34. V. Venkatesh, A. Shukla, S. Sivakumar, S. Verma, Purine-stabilized green fluorescent gold nanoclusters for cell nuclei imaging applications. ACS Appl. Mater. Interfaces **6**(3), 2185–2191 (2014)
35. H. Duan, S. Nie, Etching colloidal gold nanocrystals with hyperbranched and multivalent polymers: A new route to fluorescent and water-soluble atomic clusters. J. Am. Chem. Soc. **129**(9), 2412–2413 (2007)
36. T.-H. Chen, L. C-Y, W.-L. Tseng, One-pot synthesis of two-sized clusters for ratiometric sensing of Hg^{2+}. Talanta **117**, 258–262 (2013)

37. S. Xu, H. Yang, K. Zhao, J. Li, L. Mei, Y. Xie, A. Deng, Simple and rapid preparation of orange-yellow fluorescent gold nanoclusters using DL-homocysteine as a reducing/stabilizing reagent and their application in cancer cell imaging. RSC Adv. **5**, 11343–11348 (2015)
38. T.U.B. Rao, T. Pradeep, Luminescent Ag7 and Ag8 clusters by interfacial synthesis. Angew. Chem. Int. Ed. **49**, 3925–3929 (2010)
39. J. Zheng, C. Zhang, R.M. Dickson, Highly fluorescent, water-soluble, size-tunable gold quantum dots. Phys. Rev. Lett. **93**, 77402 (2004)
40. Y. Lu, W. Chen, Sub-nanometre sized metal clusters: From synthetic challenges to the unique property discoveries. Chem. Soc. Rev. **41**, 3594–3623 (2012)
41. X. Yuan, Z. Luo, Y. Yu, Q. Yao, J. Xie, Luminescent noble metal nanoclusters as an emerging optical probe for sensor development. Chem. Asian J. **8**, 858–871 (2013)
42. X.-H. Zhang, T.-Y. Zhou, X. Chen, Applications of metal nanoclusters in environmental monitoring. Chinese J. Anal. Chem. **43**(9), 1296–1305 (2015)
43. L. Shang, S. Dong, G.U. Nienhaus, Ultra-small fluorescent metal nanoclusters: Synthesis and biological applications. Nano Today **6**(4), 401–418 (2011)
44. L. Shang, R.M. Dörlich, S. Brandholt, R. Schneider, V. Trouillet, M. Bruns, D. Gerthsen, G.U. Nienhaus, Facile preparation of water-soluble fluorescent gold nanoclusters for cellular imaging applications. Nanoscale **3**(5), 2009–2014 (2011)
45. A. Mathew, T. Pradeep, Noble metal clusters: Applications in energy, environment, and biology. Part. Part. Syst. Charact. **31**(10), 1017–1053 (2014)
46. J. Sun, Y. Jin, Fluorescent au nanoclusters: Recent progress and sensing applications. J. Mater. Chem. C **2**, 8000–8011 (2014)
47. L. Zhang, E. Wang, Metal nanoclusters: New fluorescent probes for sensors and bioimaging. Nano Today **9**, 132–157 (2014)
48. https://www.epa.gov/ground-water-and-drinking-water/table-regulated-drinking-water-contaminants#Inorganic
49. Y. Qiao, Y. Zhang, C. Zhang, L. Shi, G. Zhang, S. Shuang, C. Dong, H. Ma, Water-soluble gold nanoclusters-based fluorescence probe for highly selective and sensitive detection of Hg^{2+}. Sens. Actuators B Chem. **224**, 458–464 (2016)
50. S. Xu, X. Li, Y. Mao, T. Gao, X. Feng, X. Luo, Novel dual ligand co-functionalized fluorescent gold nanoclusters as a versatile probe for sensitive analysis of Hg(2+) and oxytetracycline. Anal. Bioanal. Chem. **408**, 2955–2962 (2016)
51. Y. Yan, H. Yu, K. Zhang, M. Sun, Y. Zhang, X. Wang, S. Wang, Dual-emissive nanohybrid of carbon dots and gold nanoclusters for sensitive determination of mercuric ions. Nano Res. **9**(7), 2088–2096 (2016)
52. N.-Y. Hsu, Y.-W. Lin, Microwave-assisted synthesis of bovine serum albumin–gold nanoclusters and their fluorescence-quenched sensing of Hg^{2+} ions. New J. Chem. **40**, 1155–1161 (2016)
53. Y. Wang, Y. Cui, R. Liu, F. Gao, L. Gao, X. Gao, Bio-inspired peptide-Au cluster applied for mercury(II) ions detection. Sci. China Chem. **58**(5), 819–824 (2015)
54. C. Zhang, Z. Guo, G. Chen, G. Zeng, M. Yan, Q. Niu, L. Liu, Y. Zuo, Z. Huang, Q. Tan, Green-emitting fluorescence Ag clusters: Facile synthesis and sensors for Hg^{2+} detection. New J. Chem. **40**, 1175–1181 (2016)
55. D. Li, B. Li, G. Lee, S.I. Yang, Facile synthesis of fluorescent silver nanoclusters as simultaneous detection and remediation for Hg^{2+}. Bull. Kor. Chem. Soc. **36**, 1703–1706 (2015)
56. J. Peng, J. Ling, X.Q. Zhang, H.P. Bai, L. Zheng, Q.E. Cao, Z. Ding, Sensitive detection of mercury and copper ions by fluorescent DNA/Ag nanoclusters in guanine-rich DNA hybridization. Spectrochim. Acta A **137**, 1250–1257 (2015)
57. X. Liu, L. Wang, N. Zhang, D. Shangguan, Ratiometric fluorescent silver nanoclusters for the determination of mercury and copper ions. Anal. Methods **7**, 8019–8024 (2015)
58. D. Lu, Z. Chen, Y. Li, J. Yang, S. Shuang, C. Dong, Determination of mercury(II) by fluorescence using deoxyribonucleic acid stabilized silver nanoclusters. Anal. Lett. **48**, 281–290 (2015)

59. M. Xu, Z. Gao, Q. Wei, G. Chen, D. Tang, Label-free hairpin DNA-scaffolded silver nanoclusters for fluorescent detection of Hg^{2+} using exonuclease III-assisted target recycling amplification. Biosens. Bioelectron. **79**, 411–415 (2016)
60. X.-F. Wang, L.-P. Xiang, Y.-S. Wang, J.-H. Xue, Y.-F. Zhu, Y.-Q. Huang, S.-H. Chen, X. Tang, A "turn-on" fluorescence assay for lead(II) based on the suppression of the surface energy transfer between acridine orange and gold nanoparticles. Microchim. Acta **182**, 695–701 (2015)
61. Z. Yuan, M. Peng, Y. He, E.S. Yeung, Functionalized fluorescent gold nanodots: Synthesis and application for Pb^{2+} sensing. Chem. Commun. **47**, 11981–11983 (2011)
62. F. Ma, S. Liang, Y. Peng, Y. Kuang, X. Zhang, S. Chen, Y. Long, R. Zeng, Copper ion detection using novel silver nanoclusters stabilized with amido black 10B. Anal. Bioanal. Chem. **408**, 3239–3246 (2016)
63. J. Zhang, Y. Yuan, Y. Wang, F. Sun, G. Liang, Z. Jiang, Y. S-H, Microwave-assisted synthesis of photoluminescent glutathione-capped Au/Ag nanoclusters: A unique sensor-on-a-nanoparticle for metal ions, anions, and small molecules. Nano Res. **8**(7), 2329–2339 (2015)
64. H.H. Deng, L.N. Zhang, S.B. He, A.L. Liu, G.W. Li, X.H. Lin, X.H. Xia, W. Chen, Methionine-directed fabrication of gold nanoclusters with yellow fluorescent emission for Cu(2+) sensing. Biosens. Bioelectron. **65**, 397–403 (2015)
65. M. Shamsipur, F. Molaabasi, M. Shanehsaz, A.A. Moosavi-Movahedi, Novel blue-emitting gold nanoclusters confined in human hemoglobin, and their use as fluorescent probes for copper(II) and histidine. Microchim. Acta **182**, 1131–1141 (2015)
66. Y. Chang, Z. Zhang, J. Hao, W. Yang, J. Tang, BSA-stabilized au clusters as peroxidase mimetic for colorimetric detection of Ag^{+}. Sens. Actuators B Chem. **232**, 692–697 (2016)
67. Y. Yue, T.Y. Liu, H.W. Li, Z. Liu, Y. Wu, Microwave-assisted synthesis of BSA-protected small gold nanoclusters and their fluorescence-enhanced sensing of silver(I) ions. Nanoscale **4**, 2251–2254 (2012)
68. M.A.E. Francos, R. Badía-Laíño, M.E. Díaz-García, Fluorescence sensitization of gold-glutathione nanoclusters by aqueous solutions of sodium and potassium ions. Microchim. Acta **182**, 1591–1598 (2015)
69. P. Brissot, M. Ropert, C.L. Lan, O. Loreal, Non-transferrin bound iron: A key role in iron overload and iron toxicity. Biochim. Biophys. Acta **1820**, 403–410 (2012)
70. T. Chen, Y. Hu, Y. Cen, X. Chu, Y. Lu, A dual-emission fluorescent nanocomplex of gold-cluster-decorated silica particles for live cell imaging of highly reactive oxygen species. J. Am. Chem. Soc. **135**, 11595–11602 (2013)
71. S. Yang, Z. Jiang, Z. Chen, L. Tong, J. Lu, J. Wang, Bovine serum albumin-stabilized gold nanoclusters as a fluorescent probe for determination of ferrous ion in cerebrospinal fluids via the Fenton reaction. Microchim. Acta **182**, 1911–1916 (2015)
72. X. Mu, L. Qi, P. Dong, J. Qiao, J. Hou, Z. Nie, H. Ma, Facile one-pot synthesis of L-proline-stabilized fluorescent gold nanoclusters and its application as sensing probes for serum iron. Biosens. Bioelectron. **49**, 249–255 (2013)
73. J.A. Ho, H.C. Chang, W.T. Su, DOPA-mediated reduction allows the facile synthesis of fluorescent gold nanoclusters for use as sensing probes for ferric ions. Anal. Chem. **84**, 3246–3253 (2012)
74. S. Roy, G. Palui, A. Banerjee, The as-prepared gold cluster-based fluorescent sensor for the selective detection of As(III) ions in aqueous solution. Nanoscale **4**, 2734–2740 (2012)
75. J. Sun, J. Zhang, Y. Jin, 11-Mercaptoundecanoic acid directed one-pot synthesis of water-soluble fluorescent gold nanoclusters and their use as probes for sensitive and selective detection of Cr^{3+} and Cr^{6+}. J. Mater. Chem. C **1**, 138–143 (2013)
76. C.W. Wang, Y.N. Chen, B.Y. Wu, C.K. Lee, Y.C. Chen, Y.H. Huang, H.T. Chang, Sensitive detection of cyanide using bovine serum albumin-stabilized cerium/gold nanoclusters. Anal. Bioanal. Chem. **408**, 287–294 (2016)

77. N. Vasimalai, M.T. Fernandez-Arguelles, Novel one-pot and facile room temperature synthesis of gold nanodots and application as highly sensitive and selective probes for cyanide detection. Nanotechnology **27**, 475505 (2016)
78. H. Sun, D. Lu, M. Xian, C. Dong, S. Shuang, A lysozyme-stabilized silver nanocluster fluorescent probe for the detection of sulfide ions. Anal. Methods **8**, 4328–4333 (2016)
79. L. Wang, G. Chen, G. Zeng, J. Liang, H. Dong, M. Yan, Z. Li, Z. Guo, W. Tao, L. Peng, Fluorescent sensing of sulfide ions based on papain-directed gold nanoclusters. New J. Chem. **39**, 9306–9312 (2015)
80. R. Li, P. Xu, Y. Tu, J. Yan, Albumin-stabilized gold nanoclusters as viable fluorescent probes in non-titrimetric iodometry for the detection of oxidizing analytes. Microchim. Acta **183**, 497–502 (2016)
81. R. Li, P. Xu, J. Fan, J. Di, Y. Tu, J. Yan, Sensitive iodate sensor based on fluorescence quenching of gold nanocluster. Anal. Chim. Acta **827**, 80–85 (2014)
82. F. Qu, N.B. Li, H.Q. Luo, Polyethyleneimine-templated ag nanoclusters: A new fluorescent and colorimetric platform for sensitive and selective sensing halide ions and high disturbance-tolerant recognitions of iodide and bromide in coexistence with chloride under condition of high ionic strength. Anal. Chem. **84**(23), 10373–10379 (2012)
83. B. Unnikrishnan, S.C. Wei, W.J. Chiu, J. Cang, P.H. Hsu, C.C. Huang, Nitrite ion-induced fluorescence quenching of luminescent BSA-Au(25) nanoclusters: Mechanism and application. Analyst **139**, 2221–2228 (2014)
84. X. Wang, P. Wu, X. Hou, Y. Lv, An ascorbic acid sensor based on protein-modified Au nanoclusters. Analyst **138**, 229–233 (2013)
85. C.-W. Chen, C.-H. Wang, C.-M. Wei, C.-Y. Hsieh, Y.-T. Chen, Y.-F. Chen, C.-W. Lai, C.-L. Liu, C.-C. Hsieh, P.-T. Chou, Highly sensitive emission sensor based on surface plasmon enhanced energy transfer between gold nanoclusters and silver nanoparticles. J. Phys. Chem. C **114**, 799–802 (2010)
86. J.M. Liu, J.T. Chen, X.P. Yan, Near infrared fluorescent trypsin stabilized gold nanoclusters as surface plasmon enhanced energy transfer biosensor and in vivo cancer imaging bioprobe. Anal. Chem. **85**, 3238–3245 (2013)
87. X. Yan, H. Li, B. Cao, Z. Ding, X. Su, A highly sensitive dual-readout assay based on gold nanoclusters for folic acid detection. Microchim. Acta **182**, 1281–1288 (2015)
88. H. Li, Y. Cheng, Y. Liu, B. Chen, Fabrication of folic acid-sensitive gold nanoclusters for turn-on fluorescent imaging of overexpression of folate receptor in tumor cells. Talanta **158**, 118–124 (2016)
89. T. Shu, L. Su, J. Wang, C. Li, X. Zhang, Chemical etching of bovine serum albumin-protected Au_{25} nanoclusters for label-free and separation-free detection of cysteamine. Biosens. Bioelectron. **66**, 155–161 (2015)
90. X. Xu, J. Qiao, N. Li, L. Qi, S. Zhang, Fluorescent probe for turn-on sensing of L-cysteine by ensemble of AuNCs and polymer protected AuNPs. Anal. Chim. Acta **879**, 97–103 (2015)
91. Z.-X. Wang, S.-N. Ding, E.Y.J. Narjh, Determination of thiols by fluorescence using au@ag nanoclusters as probes. Anal. Lett. **48**, 647–658 (2015)
92. S. Xu, T. Gao, X. Feng, Y. Mao, P. Liu, X. Yu, X. Luo, Dual ligand co-functionalized fluorescent gold nanoclusters for the "turn on" sensing of glutathione in tumor cells. J. Mater. Chem. B **4**, 1270–1275 (2016)
93. D. Tian, Z. Qian, Y. Xia, C. Zhu, Gold nanocluster-based fluorescent probes for near-infrared and turn-on sensing of glutathione in living cells. Langmuir **28**, 3945–3951 (2012)
94. L. Hu, S. Han, S. Parveen, Y. Yuan, L. Zhang, G. Xu, Highly sensitive fluorescent detection of trypsin based on BSA-stabilized gold nanoclusters. Biosens. Bioelectron. **32**, 297–299 (2012)
95. G.L. Wang, L.Y. Jin, Y.M. Dong, X.M. Wu, Z.J. Li, Intrinsic enzyme mimicking activity of gold nanoclusters upon visible light triggering and its application for colorimetric trypsin detection. Biosens. Bioelectron. **64**, 523–529 (2015)
96. X. Jiang, D.-Q. Feng, G. Liu, D. Fan, W. Wang, A fluorescent switch sensor for detection of anticancer drug and ctDNA based on the glutathione stabilized gold nanoclusters. Sens. Actuators B Chem. **232**, 276–282 (2016)

97. Y. Zhu, X.C. Hu, S. Shi, R.R. Gao, H.L. Huang, Y.Y. Zhu, X.Y. Lv, T.M. Yao, Ultrasensitive and universal fluorescent aptasensor for the detection of biomolecules (ATP, adenosine and thrombin) based on DNA/Ag nanoclusters fluorescence light-up system. Biosens. Bioelectron. **79**, 205–212 (2016)
98. P.H. Li, J.Y. Lin, C.T. Chen, W.R. Ciou, P.H. Chan, L. Luo, H.Y. Hsu, E.W. Diau, Y.C. Chen, Using gold nanoclusters as selective luminescent probes for phosphate-containing metabolites. Anal. Chem. **84**, 5484–5488 (2012)
99. S. Liu, H. Wang, Z. Cheng, H. Liu, Facile synthesis of near infrared fluorescent trypsin-stabilized Ag nanoclusters with tunable emission for 1,4-dihydronicotinamide adenine dinucleotide and ethanol sensing. Anal. Chim. Acta **886**, 151–156 (2015)
100. L.Y. Chen, C.C. Huang, W.Y. Chen, H.J. Lin, H.T. Chang, Using photoluminescent gold nanodots to detect hemoglobin in diluted blood samples. Biosens. Bioelectron. **43**, 38–44 (2013)
101. X. Chen, G.A. Baker, Cholesterol determination using protein-templated fluorescent gold nanocluster probes. Analyst **138**, 7299–7302 (2013)
102. J. Wang, Y. Chang, W.B. Wu, P. Zhang, S.Q. Lie, C.Z. Huang, Label-free and selective sensing of uric acid with gold nanoclusters as optical probe. Talanta **152**, 314–320 (2016)
103. P. Xu, R. Li, Y. Tu, J. Yan, A gold nanocluster-based sensor for sensitive uric acid detection. Talanta **144**, 704–709 (2015)
104. Y. Tao, Y. Lin, J. Ren, X. Qu, A dual fluorometric and colorimetric sensor for dopamine based on BSA-stabilized Au nanoclusters. Biosens. Bioelectron. **42**, 41–46 (2013)
105. Y. Teng, X. Jia, J. Li, E. Wang, Ratiometric fluorescence detection of tyrosinase activity and dopamine using thiolate-protected gold nanoclusters. Anal. Chem. **87**, 4897–4902 (2015)
106. J. Sun, F. Yang, X. Yang, Synthesis of functionalized fluorescent gold nanoclusters for acid phosphatase sensing. Nanoscale **7**, 16372–16380 (2015)
107. Y. Xu, P.E. Pehrsson, L. Chen, R. Zhang, W. Zhao, Double-stranded DNA single-walled carbon nanotube hybrids for optical hydrogen peroxide and glucose sensing. J. Phys. Chem. C **111**, 8638–8643 (2007)
108. J. Lu, R.F. Bu, Z.L. Sun, Q.S. Lu, H. Jin, Y. Wang, S.H. Wang, L. Li, Z.L. Xie, B.Q. Yang, Comparable efficacy of self-monitoring of quantitative urine glucose with self-monitoring of blood glucose on glycaemic control in non-insulin-treated type 2 diabetes. Diabetes Res. Clin. Pract. **93**, 179–186 (2011)
109. X. Jiang, C. Sun, Y. Guo, G. Nie, L. Xu, Peroxidase-like activity of apoferritin paired gold clusters for glucose detection. Biosens. Bioelectron. **64**, 165–170 (2015)
110. L. Jin, L. Shang, S. Guo, Y. Fang, D. Wen, L. Wang, J. Yin, S. Dong, Biomolecule-stabilized au nanoclusters as a fluorescence probe for sensitive detection of glucose. Biosens. Bioelectron. **26**, 1965–1969 (2011)
111. L.-L. Wang, J. Qiao, L. Qi, X.-Z. Xu, D. Li, Construction of OVA-stabilized fluorescent gold nanoclusters for sensing glucose. Sci. China Chem. **58**(9), 1508–1514 (2015)
112. X. Xia, Y. Long, J. Wang, Glucose oxidase-functionalized fluorescent gold nanoclusters as probes for glucose. Anal. Chim. Acta **772**, 81–86 (2013)
113. F. Wen, Y. Dong, L. Feng, S. Wang, S. Zhang, X. Zhang, Horseradish peroxidase functionalized fluorescent gold nanoclusters for hydrogen peroxide sensing. Anal. Chem. **83**, 1193–1196 (2011)
114. M. Dasog, R.W.J. Scott, Understanding the oxidative stability of gold monolayer-protected clusters in the presence of halide ions under ambient conditions. Langmuir **23**, 3381–3387 (2007)
115. Y.C. Shiang, C.C. Huang, H.T. Chang, Gold nanodot-based luminescent sensor for the detection of hydrogen peroxide and glucose. Chem. Commun. **23**, 3437–3439 (2009)
116. T. Das, D.K. Poria, P. Purkayastha, NIR-emitting chiral gold nanoclusters coated with γ-cyclodextrin are pH sensitive: Application as biomarker. Nanomed. Nanotech. Biol. Med. **12**, 1105–1112 (2016)

117. C. Ding, Y. Tian, Gold nanocluster-based fluorescence biosensor for targeted imaging in cancer cells and ratiometric determination of intracellular pH. Biosens. Bioelectron. **65**, 183–190 (2015)
118. C.Y. Ke, Y.T. Wu, W.L. Tseng, Fluorescein-5-isothiocyanate-conjugated protein-directed synthesis of gold nanoclusters for fluorescent ratiometric sensing of an enzyme-substrate system. Biosens. Bioelectron. **69**, 46–53 (2015)
119. W. Song, Y. Wang, R.-P. Liang, L. Zhang, J.-D. Qiu, Label-free fluorescence assay for protein kinase based on peptide biomineralized gold nanoclusters as signal sensing probe. Biosens. Bioelectron. **64**, 234–240 (2015)
120. L. Qin, X. He, L. Chen, Y. Zhang, Turn-on fluorescent sensing of glutathione S-transferase at near-infrared region based on FRET between gold nanoclusters and gold nanorods. ACS Appl. Mater. Interfaces **7**(10), 5965–5971 (2015)
121. H. Li, Y. Guo, L. Xiao, B. Chen, Selective and sensitive detection of acetylcholinesterase activity using denatured protein-protected gold nanoclusters as a label-free probe. Analyst **139**, 285–289 (2014)
122. W.Y. Chen, L.Y. Chen, C.M. Ou, C.C. Huang, S.C. Wei, H.T. Chang, Synthesis of fluorescent gold nanodot-liposome hybrids for detection of phospholipase C and its inhibitor. Anal. Chem. **85**, 8834–8840 (2013)
123. Y. Chen, H. Zhou, Y. Wang, W. Li, J. Chen, Q. Lin, C. Yu, Substrate hydrolysis triggered formation of fluorescent gold nanoclusters-A new platform for the sensing of enzyme activity. Chem. Commun. **49**, 9821–9823 (2013)
124. Y. Chen, W. Li, Y. Wang, X. Yang, J. Chen, Y. Jiang, C. Yu, Q. Lin, Cysteine-directed fluorescent gold nanoclusters for the sensing of pyrophosphate and alkaline phosphatase. J. Mater. Chem. C **2**, 4080–4085 (2014)
125. Y. Wang, Y. Wang, F. Zhou, P. Kim, Y. Xia, Protein-protected Au clusters as a new class of nanoscale biosensor for label-free fluorescence detection of proteases. Small **8**(24), 3769–3773 (2012)
126. Z. Tan, H. Xu, G. Li, X. Yang, M.M. Choi, Fluorescence quenching for chloramphenicol detection in milk based on protein-stabilized Au nanoclusters. Spectrochim. Acta A **149**, 615–620 (2015)
127. K. Chatterjee, C.W. Kuo, A. Chen, P. Chen, Detection of residual rifampicin in urine via fluorescence quenching of gold nanoclusters on paper. J. Nanobiotechnol. **13**, 46 (2015). https://doi.org/10.1186/s12951-015-0105-5
128. Z. Li, Y. Wang, Y. Ni, S. Kokot, Fluorescence analysis of 6-mercaptopurine with the use of a nano-composite consisting of BSA-capped Au nano-clusters and core-shell $Fe_3O_4SiO_2$ nanoparticles. Biosens. Bioelectron. **70**, 246–253 (2015)
129. P. Wang, B.L. Li, N.B. Li, H.Q. Luo, A fluorescence detection of D-penicillamine based on Cu(2+)-induced fluorescence quenching system of protein-stabilized gold nanoclusters. Spectrochim. Acta A **135**, 198–202 (2015)
130. J. Wang, Y. Chang, P. Zhang, S.Q. Lie, P.F. Gao, C.Z. Huang, Cu(2+)-mediated fluorescence switching of gold nanoclusters for the selective detection of clioquinol. Analyst **140**, 8194–8200 (2015)
131. X. Wang, P. Wu, Y. Lv, X. Hou, Ultrasensitive fluorescence detection of glutaraldehyde in water samples with bovine serum albumin-Au nanoclusters. Microchem. J. **99**, 327–331 (2011)
132. Z. Chen, S. Qian, X. Chen, W. Gao, Y. Lin, Protein-templated gold nanoclusters as fluorescence probes for the detection of methotrexate. Analyst **137**, 4356–4361 (2012)
133. T. Zhao, Z.-Q. Xuan, A. Wan, R. Gui, Bovine serum albumin template synthesis of fluorescent gold nanoclusters for nitric oxide detection in vitro. Mater. Technol. **31**(6), 342–347 (2016)
134. X. Liu, C. Fu, X. Ren, H. Liu, L. Li, X. Meng, Fluorescence switching method for cascade detection of salicylaldehyde and Zinc(II) ion using protein protected gold nanoclusters. Biosens. Bioelectron. **74**, 322–328 (2015)
135. L.V. Nair, D. Philips, R. Jayasree, A. Ajayaghosh, A near-infrared fluorescent nanosensor (AuC@Urease) for the selective detection of blood urea. Small **9**(16), 2673–2677 (2013)

136. C.L. Zheng, Z.X. Ji, J. Zhang, S.N. Ding, A fluorescent sensor to detect sodium dodecyl sulfate based on the glutathione-stabilized gold nanoclusters/poly diallyldimethylammonium chloride system. Analyst **139**, 3476–3480 (2014)
137. S. Wanga, P. Liua, Y. Qinb, Z. Chena, J. Shen, Rapid synthesis of protein conjugated gold nanoclusters and their application in tea polyphenol sensing. Sens. Actuators B Chem. **223**, 178–185 (2016)
138. C.L. Gopu, A.S. Krishna, K. Sreenivasan, Fluorimetric detection of hypochlorite using albumin stabilized gold nanoclusters. Sens. Actuators B Chem. **209**, 798–802 (2015)
139. H. Dai, Y. Shi, Y. Wang, Y. Sun, J. Hu, P. Ni, Z. Li, Label-free turn-on fluorescent detection of melamine based on the anti-quenching ability of Hg^{2+} to gold nanoclusters. Biosens. Bioelectron. **53**, 76–81 (2014)
140. X. Yang, J. Wang, D. Su, Q. Xia, F. Chai, C. Wang, F. Qu, Fluorescent detection of TNT and 4-nitrophenol by BSA Au nanoclusters. Dalton Trans. **43**, 10057–10063 (2014)
141. X. Wu, Z. Zhang, J. Li, H. You, Y. Li, L. Chen, Molecularly imprinted polymers-coated gold nanoclusters for fluorescent detection of bisphenol A. Sens. Actuators B Chem. **211**, 507–514 (2015)
142. D. Cheng, M. Yu, F. Fu, W. Han, G. Li, J. Xie, Y. Song, M.T. Swihart, E. Song, Dual recognition strategy for specific and sensitive detection of bacteria using aptamer-coated magnetic beads and antibiotic-capped gold nanoclusters. Anal. Chem. **88**, 820–825 (2016)
143. J. Liu, L. Lu, S. Xu, L. Wang, One-pot synthesis of gold nanoclusters with bright red fluorescence and good biorecognition abilities for visualization fluorescence enhancement detection of *E. coli*. Talanta **134**, 54–59 (2015)
144. P.H. Chan, Y.C. Chen, Human serum albumin stabilized gold nanoclusters as selective luminescent probes for *Staphylococcus aureus* and methicillin-resistant *Staphylococcus aureus*. Anal. Chem. **84**, 8952–8956 (2012)
145. C.C. Huang, C.T. Chen, Y.C. Shiang, Z.H. Lin, H.T. Chang, Synthesis of fluorescent carbohydrate-protected Au nanodots for detection of Concanavalin A and *Escherichia coli*. Anal. Chem. **81**, 875–882 (2009)
146. Y.-T. Tseng, R. Cherng, Z. Yuan, C.-W. Wu, H.-T. Chang, C.-C. Huang, Ultrasound-mediated modulation of the emission of gold nanodots. Nanoscale **8**, 5162–5169 (2016)